Phase Transition Phenomena in Quantum Spin Systems and in Polyampholyte Gels

by

Daniel Paul Aalberts

B.S., Physics
Massachusetts Institute of Technology, 1989.

Submitted to the Department of Physics
in partial fulfillment of the requirements for the degree of

Doctor of Philosophy

at the

MASSACHUSETTS INSTITUTE OF TECHNOLOGY

September 1994

Author .....
Department of Physics
August 5, 1994

Certified by .....
A. Nihat Berker
Professor of Physics
Thesis Supervisor

Accepted by .....
George F. Koster
Professor of Physics
Chairman, Departmental Committee on Graduate Students

Phase Transition Phenomena in Quantum Spin Systems and in Polyampholyte Gels

by

Daniel Paul Aalberts

Submitted to the Department of Physics
on August 5, 1994, in partial fulfillment of the
requirements for the degree of
Doctor of Philosophy

Abstract

We use the Suzuki-Trotter (ST) transformation to map exactly fully quantum mechanical Hamiltonians in d-dimensions to a classical system in $(d+1)$-dimensions. We study the two-dimensional classical Ising model that is equivalent, via the ST mapping, to the XXZ-Heisenberg quantum-spin chain. By imposing appropriate boundary conditions to the Ising model, the spin waves of the quantum model are studied. We reproduce the entire energy spectrum of the two-spin-wave states and derive bound-state energies of the three-spin-wave states.

Next, I use the ST mapping to study the fully quantum mechanical XY model in two dimensions. In the equivalent classical model, the phase transition is intuitively described and new order parameters are invented. A Monte Carlo (MC) study confirms that this picture's transition takes the Kosterlitz-Thouless form. Two additional local symmetries which have, to date, been neglected in Quantum Monte Carlo simulations are revealed and used.

Next we study phase behavior in gels. The newly developed Bond Fluctuation Method (BFM) allows cross-linked polymer networks to be studied via Monte Carlo simulation. I study the scaling behavior of gels, determining the scaling exponent ν in two and three dimensions. The distance between cross-links follows the scaling law for self-avoiding random walks, $R_{\mathrm{L}} \sim N^{\nu}$, which confirms a supposition of Flory.

Tanaka and colleagues showed that ionic gels, which are composed of acidic monomer units, exist in expanded or collapsed phases. Two interactions — the quality of the solvent and the work done by a gas of counterions — suffice to characterize the first-order phase transition in these BFM simulations in two dimensions. A technique is introduced which prevents local attractive interactions from hindering global relaxation.

Recent experiments by Annaka and Tanaka have yielded multiple coexistence loops for gels with random positive and negative ionic groups, demonstrating the existence of up to seven distinct macroscopic phases distinguished by volume discontinuities. We introduce for this system a microscopic model in which the randomness translates into random fields resulting in competing quenched random interactions in

a spin system. The many phases observed in this model are similar to the experimental results and are understood as randomly coordinated phases.

Thesis Supervisor: A. Nihat Berker
Title: Professor of Physics

Acknowledgments

I thank my advisor Professor A. Nihat Berker for suggesting interesting problems, for giving me the freedom to follow my nose to make them my own, for guidance when I needed it, and for insisting on good work and clear presentation. His drive for excellence has been inspiring. ("Until you're dead there is always one more neuron which you can make scream.") I met Nihat when I was an undergraduate taking his introductory solid state physics course. His ability to explain clearly and intuitively led me to work with him and I have enjoyed learning from him since then.

I thank Professor John Joannopoulos for agreeing to be a reader for this thesis, for helpful advice, for brilliant teaching, and for coming to see my plays from time to time. I thank Professor Toyo Tanaka for agreeing to read my thesis and for doing so many interesting experiments.

I thank my colleagues Alexis Falicov, Bill Hoston, Roland Netz, Bob Meade, Pierre Villeneuve, Maureen Fahey, Charlie Collins, and Michael Schwartz for their camaraderie, invaluable insights, and thoughtful comments and suggestions. I also thank my office-mates Alkan Kabakçıoğlu and Ricardo Paredes for a year of pleasant conversations. I thank Fred Hicks for making organic chemistry so interesting and for supplying correct pK_a values off the top of his head.

I am grateful to my friends in the arts who have helped make graduate school enjoyable; particularly Dr. Alton Bynum, Larry Taylor, Dave Darmofal, Terry Alkasab, Liz Kujawinski, Michael Ouellette, Jeannette Ryan and Tom Woodman.

I thank Tony Gray for friendship, lunches, and for offering to write me into a book.

I thank my parents and my brother for a lifetime of love and support.

I thank Danielle for making my life wonderful and letting me love her. Thank you for sharing this adventure and for coming with me on the next.

This research was supported by the U.S. Department of Energy Grant No. DE-FG02-92ER45473, U.S. National Science Foundation Grant No. DMR-90-22933, and by a U.S. National Science Foundation Graduate Fellowship.

Contents

List of Figures

List of Tables

Chapter 1

Introduction

The Principle of Universality tells us that for a wide variety of physical systems the order parameter behaves in the same way when the underlying symmetry of the microscopic interactions is the same. An order parameter is an experimentally measurable quantity which distinguishes phases of matter. Order generally increases as the temperature is reduced; for example, molecules in the gas phase are unbound and free to move around while in the liquid phase molecules are loosely bound to ever-changing neighbors while molecules in the solid phase are frozen into fixed relation to their neighbors.

Two commonly known phase diagrams are water's solid-liquid-gas phase diagram [Fig. 1-1(a)] and the phase diagram of a ferromagnet [Fig. 1-1(b)]. Increasing the temperature at one atmosphere of pressure changes ice to liquid water and later to water vapor (steam). The density of water changes discontinously at the transitions at that pressure; such discontinuous transitions are called "first order." At the transition, the two phases coexist; for example, ice cubes can sit in a glass of water at the freezing temperatures.

Note that the liquid-vapor line terminates in a point labelled C at high pressure and high temperature. High pressure increases the density of the gas phase and high temperature decreases the density of the liquid phase. The difference between the densities of the two phases decreases until eventually it goes to zero at point C. Point C is an example of a "second-order transition" or "critical" point.

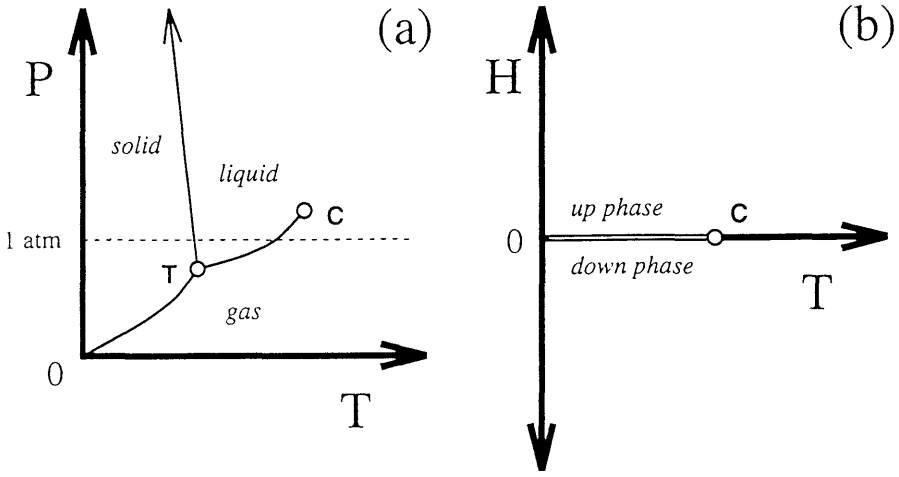

Figure 1-1: (a) Schematic phase diagram for water plotted against pressure and temperature. The solid lines indicate discontinuous or "first-order" phase boundaries between the solid, liquid, and gas phases. The point labelled T is the triple-point where all phases can coexist. The point labelled C is a critical point, where transitions are continuous. The phase diagram of a ferromagnet is depicted in (b). The first-order boundary extends from zero temperature to the critical point C.

Passing through critical points or second-order lines, the order parameter (in this case, the difference between the densities of the liquid and vapor phases) changes rapidly though not discontinuously. Fluctuations in observables are generally greatest at critical points.

The Ising-type ferromagnet phase diagram [Fig. 1-1(b)] is qualitatively similar to the liquid-gas region of Fig. 1-1(a). As depicted in Fig. 1-1(b), at high temperature there is no net magnetic moment but at low temperature the ferromagnet spontaneously magnetizes in one of two directions. If a field H is applied in the direction opposite to the magnetization, the magnet will eventually realign with a marked change of magnetization. The order parameter for this system is half the difference between the magnetization of the up and down phases at $H = 0$.

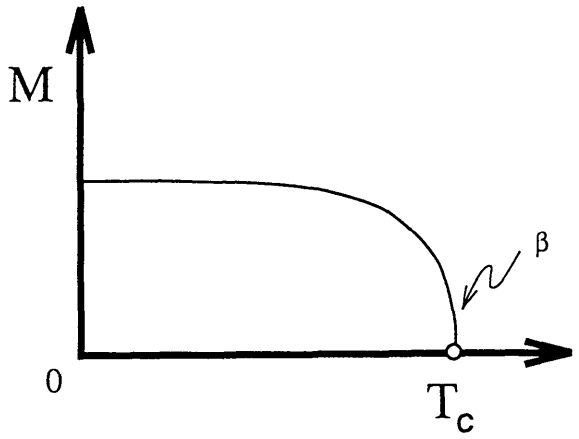

Figure 1-2: The magnetization M which is the order parameter for ferromagnets is plotted as a function of temperature. Above the critical temperature, thermal fluctuations destroy ferromagnetism. The system magnetizes at low temperature. The "critical exponent" β characterizes the growth in the order parameter near T_C.

As depicted in Fig. 1-2, the order parameter behaves as a power law of the distance from the critical temperature

$$M \sim \left(\frac{T_c - T}{T_c}\right)^{\beta}. \tag{1.1}$$

In Eq. 1.1, I have used the notation of magnetism (the net magnetic moment M is the order parameter); β is the order parameter critical exponent. There are different sets of critical exponents — *eg:* $\{\beta, \alpha, \nu, \ldots\}$ — as there are different underlying symmetries and space dimensionalities. The definitions for various exponents are given in Stanley's book.[1]

Let's return to first-order transitions of Fig. 1-1. When one passes through a first-order transition faster than the system can respond and reach the new global equilibrium phase, hysteresis is observed.

[1] H.E. Stanley, *Introduction to Phase Transitions and Critical Phenomena*, (Oxford Univ. Press, New York, 1971).

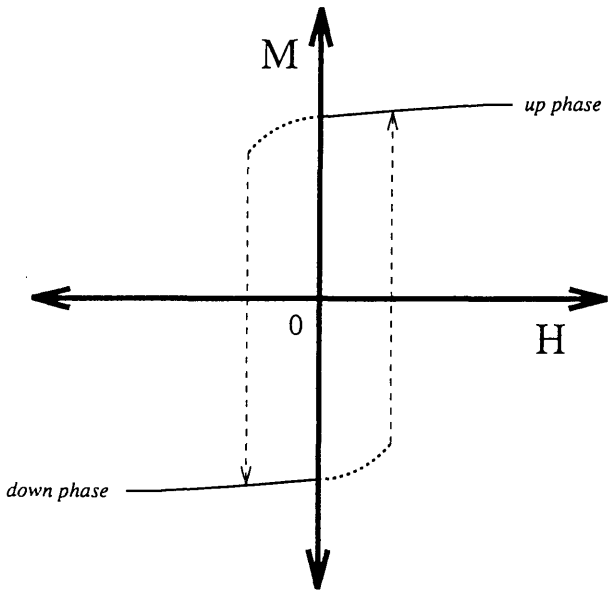

Figure 1-3: The magnetization M is plotted as a function of applied field H. The solid curve labels equilibrium phases (up and down), dashed curves labels how a phase can extend across a first-order transition boundary into the other phase's domain before eventually collapsing to the true equilibrium phase.

Figure 1-3 shows that if one applies a field H to change phases through a first-order transition, often the initial phase persists into the final phase. This behavior is well-known for magnets, and weatherpersons know hysteresis as "supersaturation" when the relative humidity temporarily but measurably exceeds 100% before rainfall. When hysteresis is pronounced, the observed state of the system can depend strongly on the thermodynamic path taken to the final temperature and field.

Successful theories for these systems have been built around classical (n-component vector with commuting operators) representations of the local variables.[2]

On the smallest length scales, however, matter interacts according to the rules of quantum mechanics so representing the local variables as n-component real vectors which commute is not truly accurate.

Quantum mechanics complicates calculations and intuitions because there is a quantum operator, in place of a classical vector, to represent some local magnetic

[2] *Phase Transitions and Critical Phenomena*, edited by C. Domb, M.S. Green, and J.L. Lebowitz (Academic Press, New York, 1976-1994).

moment; only the quantized value of the moment in some basis can be known.

What makes quantum mechanics so intuitively unnatural is that a spin which would be represented classically as a vector in three-space an take (for $S = 1/2$) only two discrete values — called the "+" and "−" states — along the measurement direction. The other level of complexity that quantum mechanics introduces arises from the non-commutivity of operators; the result of an observation can change depending on the order in which quantum measurements are made.

We were interested in solving problems in statistical physics that fully incorporate quantum mechanics into model Hamiltonians. To attack quantum statistical mechanics problems, we follow Suzuki who employs an exact identity of Trotter's for mapping a quantum problem in d dimensions to a classical (commuting operators) system with somewhat complicated — but local — interactions in one additional dimension. One great advantage to working with the $(d + 1)$-dimensional system is that the local variables take values of ± 1 and commute (as long as local constraints are satisfied) which enables computer simulations as well as rigorous mathematics. The Quantum Monte Carlo (QMC) technique popularized by Suzuki has allowed investigators to accurately study properties of quantum Hamiltonians.[3]

We studied the excitation spectrum of the spin wave problem working within the Suzuki-Trotter (ST) formalism without resorting to QMC. This work is presented in Sec. 2.1. In this model, X and Y components of quantum spins ($S = 1/2$) interact with the same interaction strength K while the Z component coupling K_z may be different. The excitation spectrum for small deviations from the fully aligned state (which is the ground state for $K_z \geq K$) was calculated in this formalism. Exact solutions are obtained in agreement with previously published results derived from another technique, namely the Bethe *ansatz*. New results are also obtained.

To verify that correctly including the quantum interactions does not effect the universality of phase transitions I studied the quantum XY model which is presented in Sec. 2.2. Other investigators have used QMC to show that the Principle of Universality extends to quantum systems. The most successful of these calculated correlation

[3] *Quantum Monte Carlo Methods*, edited by M. Suzuki (Springer-Verlag, Berlin, 1987).

functions for large systems and showed that their results agreed with the classical theories. One difficulty with these approaches is that there is no convenient intuitive mental picture of what is happening to the quantum spins which distinguishes the disordered phase from the low temperature phase.

A general picture of how local variables look in different phases emerges and helps in our understanding of the transition. One example is the liquid to vapor transition where one can picture molecules being compressed by high pressure into the liquid form on the one hand, but being impelled to fly apart by thermal energy on the other; another example is the magnetic case where one can imagine that vector magnetic moments want to align but thermal energy seeks to randomize them; yet another example is Kosterlitz and Thouless' picture of the binding and unbinding transition of topological defects called vortices.

In Sec. 2.2, I show that in the ST formalism, there is an intuitive way of understanding the quantum XY phase transition. I hope that this visual/intuitive way of looking at the problem may allow some of the renormalization-group techniques to be used effectively. The renormalization-group procedure requires the amalgamation of local quantities (spins) into macro-spins and calculating the effective couplings on progressively larger length scales; therefore, one must first learn how to combine quantum spins into macro-quantum spins.

Another interesting research area in statistical physics — how randomness effects phase behavior — is explored in Chapter 3. Because many of the solved models are highly idealized, it is important to know whether real materials with random imperfections will behave in the same universality class as the theoretical ideal predicts. That is, in part, the subject of my colleague Alexis Falicov's doctoral work.

Random systems are also particularly interesting because they present a starting point for studying the complex interactions of proteins or DNA. Often, one is interested in how random competing interactions can lead to multiple stable configurations and thus multiple observable phases. Statistical physicists often study these types of systems under the name "spin-glasses."

Proteins are polymer chains with different monomeric groups which interact with

competing Coulombic, hydrogen-bonding, and hydrophobic–hydrophilic interactions. These interactions, for particular chain sequences, lead to uniquely folded structures which act as catalysts for biologically important reactions. One puzzle concerns why particular sequences have biological relevance while the vast majority of sequences do not.

A logical starting place in an effort to solve this puzzle is to study gels made up of random monomer sequences to distinguish the behavior of purely random systems from what you would see using special sequences. Professor Tanaka's group at MIT lately has also been interested in creating "smart gels" which use receptors on the gel or other means to induce a phase transition to perform a useful function. One such system is a gel which undergoes a phase transition when saccharides are present[4] and therefore serves a diagnostic function.

In Chapter 3 of this thesis, I study systems in which random interactions play an important role: polyampholyte gels. The term "polyampholyte" refers to polymer chains with monomers (the links in the chain) composed of acidic *and* basic components. Unlike polyelectrolytes which have only acidic *or* only basic monomers and are swollen by self-repulsion, attractive Coulombic interactions may dominate in polyampholytes, leading to a collapsed phase. Polymer chains are hooked together by multi-functional units called "cross-links" or "branch points" to make a random, globally connected network. Experiments conducted by Professor Tanaka's group on polyampholyte gels showed a very rich phase behavior with many stable configurations at given external conditions (*i.e.*, temperature and pH).

Two programs of investigation are used here for studying gels: In the first program (Secs. 3.1 and 3.2), a Monte Carlo simulation technique called the Bond Fluctuation Method (BFM) is used to study model gels. Using the BFM, I first study how the volume of gels and the lengths of the polymer chains in gels scale with the number of links in the chain. Then, I introduce into the BFM simulation interactions between the gel and the solvent to simulate the phase transition in ionic (polyelectrolytic) gels. In experiments conducted by Tanaka and colleagues on ionic gels, only two phases —

[4]E. Kokufata, Y.-Q. Zhang, and T. Tanaka, Nature **351**, 302 (1991).

swollen and collapsed — were observed. The swollen phase is the gel analog of the vapor phase; the collapsed phase, of the liquid phase.

In the second program of investigation (Sec. 3.3), we model gels composed of randomly distributed monomer types (acidic or basic) subject to Coulomb interactions. For $\mathrm{pH} \gtrless \mathrm{pK_a}$, acidic monomers are predominantly ionized or neutral while for $\mathrm{pH} \lesseqgtr \mathrm{pK_b}$, basic monomers are predominantly ionized or neutral. For these experiments, there is a pH region where *both* types are ionized and in this region oppositely charged groups can form ionic bonds, reducing the size of the gel. We consider coupled density and charge local variables in our model Hamiltonian and achieve good qualitative agreement with novel experimental results.

Finally, in Chapter 4, I present my conclusions and a look to the future.

Chapter 2

Quantum Systems

In this chapter, I describe two quantum statistical mechanics calculations entitled: "Spin-Wave Bound-State Energies from an Ising Model" and "Entanglement Transition in the Two-Dimensional Quantum XY Model." Both employ the Suzuki-Trotter formalism to map a spin-$\frac{1}{2}$ problem in d dimensions onto a classical problem in $(d+1)$-dimensions.

2.1 Spin-Waves

The first system studied is the quantum XXZ-chain. Bethe calculated the excitation spectrum of single spin-deviations and two spin-deviations in the Heisenberg case in which X,Y, and Z couplings are equal. The Heisenberg Hamiltonian is

$$\mathcal{H} = -A \sum_n \sigma_n \cdot \sigma_{n+1}, \tag{2.1}$$

where σ denotes the Pauli spin matrices.

A clear treatment of Bethe's solution is given by Feynman.[1] I shall summarize Bethe's results. A ferromagnetic ground-state is one in which all of the spins are aligned; for example, $|+++\cdots+\rangle$. For single-spin deviations, the eigenfunctions are

[1] R.P. Feynman, *Statistical Mechanics: A Set of Lectures*, (Benjamin/Cummings Publishing Company, Reading Massachussetts, 1972), Chapter 7.

Fourier transforms of kets labelling the site with the minus spin.

$$|k\rangle = \sum_n e^{ikn}|n\rangle, \tag{2.2}$$

with $|n\rangle$ denoting a spin-deviation $(-)$ at site n. The spin-wave energy relative to the fully aligned state is

$$E = 4A(1 - \cos k). \tag{2.3}$$

Bethe also considered the case of two-spin deviations. He realized that it is energetically favorable for two-spin deviations to sit next to each other — one less bond is broken — and that spin-wave bound-states were possible. He solved for complete energy spectrum of two spin-deviations with an *ansatz* for bound and unbound wavefunctions. In his approach, an amplitude is assigned to unphysical kets, namely those states in which two-spin deviations are assigned to the same site. Doing this eliminates one equation at the expense of an additional constraint on the wavefunctions which is satisfied by his *ansatz*. His approach can be generalized to more spin deviations although it becomes progressively more complicated to solve.

In the following paper, "Spin-Wave Bound-State Energies from an Ising Model," we study a slightly more general Hamiltonian than Eq. 2.1, the quantum XXZ-chain. This published work may be found in Phys. Rev. B **49**, 1073 (1994). We use the Suzuki-Trotter mapping to map this quantum problem in one dimension to a (1+1)-dimensional classical problem and calculate energy spectra including the three spin-wave bound states. The calculation proceeds without assigning amplitudes to unphysical kets.

Spin-Wave Bound-State Energies from an Ising Model

Daniel P. Aalberts and A. Nihat Berker

Department of Physics, Massachusetts Institute of Technology, Cambridge, Massachusetts 02139

Abstract

We study the two-dimensional classical Ising model that is equivalent, via the Suzuki-Trotter mapping, to the XXZ Heisenberg quantum-spin chain. By imposing appropriate boundary conditions to the Ising model, the spin waves of the quantum model are studied. We reproduce the entire energy spectrum of the two-spin-wave states and derive bound-state energies of the three-spin-wave states. Thus, the continuum energetics of the elementary excitations of a d-dimensional quantum model are contained in the equivalent $(d+1)$-dimensional classical model, even though the latter is a discrete-spin model.

PACS Numbers: 75.30.Ds, 03.65.Ge, 05.30.Ch, 64.60.Cn

I. Introduction

Noncommuting quantum-mechanical operators bring an added degree of difficulty to the statistical-mechanical treatment of model systems. A general step along the direction of relieving this difficulty was taken by Suzuki [1], who showed that the Trotter formula [2] can be employed to map, rigorously, d-dimensional quantum-mechanical systems onto $(d+1)$-dimensional classical systems with somewhat complicated, but local, interactions and constraints. This mapping for the partition function is similar to the Feynman path-integral formalism for particle propagators in many-body theory. The Suzuki-Trotter transformation has to date been exploited to enable Monte Carlo simulations, which are carried out on the equivalent $(d+1)$-dimensional classical system [3, 4, 5, 6]. Unfortunately, it has not been much used within closed-form treatments of model systems.

The classical system that is the upshot of the Suzuki-Trotter mapping is composed of discrete, namely Ising-type, local degrees of freedom. Therefore, a question that arises is how the latter system incorporates elementary excitations of the initial quantum-mechanical system such as spin waves, that have a continuously varying energy spectrum. We have investigated this question with XXZ Heisenberg magnetic chains. We find that its answer lies, quite generally, in the extreme spatial anisotropy of the $(d+1)$-dimensional classical system. In the process of this study, working with the equivalent classical Ising system, we have reproduced the entire energy spectrum of the two-spin-wave quantum states and we have derived bound-state energies of the three-spin-wave quantum states.

II. The XXZ Heisenberg Magnetic Chain and Its Equivalent Classical Ising Model

The XXZ Heisenberg chain is defined by the Hamiltonian

$$-\beta\mathcal{H}_{XXZ} = K\sum_i(\sigma_i^x\sigma_{i+1}^x + \sigma_i^y\sigma_{i+1}^y) + K_z\sum_i\sigma_i^z\sigma_{i+1}^z, \tag{2.4}$$

where $\beta = 1/k_B T$, and σ_i^u are the Pauli spin matrices at site i. For $K = K_z$, $0 < |K| < |K_z|$, $|K| > |K_z| > 0$, $K = 0 \neq K_z$, and $K \neq 0 = K_z$ the model respectively reduces to the Heisenberg, easy-axis Heisenberg, easy-plane Heisenberg, Ising, and XY models. This model has been treated by Bethe [7], Dyson [8], Orbach [9], Wortis [10], and others, within its quantum-mechanical formulation.

Suzuki has mapped [1] the XXZ chain onto a classical system as follows. The Hamiltonian is separated into two terms, each containing every other bond. The Trotter formula states that

$$e^{-\beta\mathcal{H}_1 - \beta\mathcal{H}_2} = \lim_{n\to\infty} \left(e^{-\beta\mathcal{H}_1/n} e^{-\beta\mathcal{H}_2/n}\right)^n, \tag{2.5}$$

the corrections being of order n^{-1}. Suzuki uses this formula by inserting a complete set of states between each of the $2n$ factors in the right side. In each $-\beta\mathcal{H}_j/n$, the operators associated with a given bond $(i, i+1)$ commute with all other operators. Thus, the matrix elements, resulting from the insertion of the complete set of states, themselves factorize to local calculations of matrix elements of single-bond operators. The result of such a calculation amounts to a local coupling in a classical two-dimensional Hamiltonian, where the degrees of freedom are the quantum numbers of the single-bond operators in two adjoining inserted states.

The equivalent classical $d = 2$ anisotropic model is finalized, after the insertion of states and the calculations just mentioned, by taking matrix elements of the operator in Eq. (2.5), in manners to be specified in Sec. III, which determines the classical boundary conditions. The resulting model is composed of classical spins $m_{i,j} = \pm 1$ at each site (i, j) of a square lattice. These classical spins are coupled by local interactions that are grouped into every other square in a checkerboard pattern, as shown in Fig. 2-1. Thus, in this figure, each darkened square contributes to the

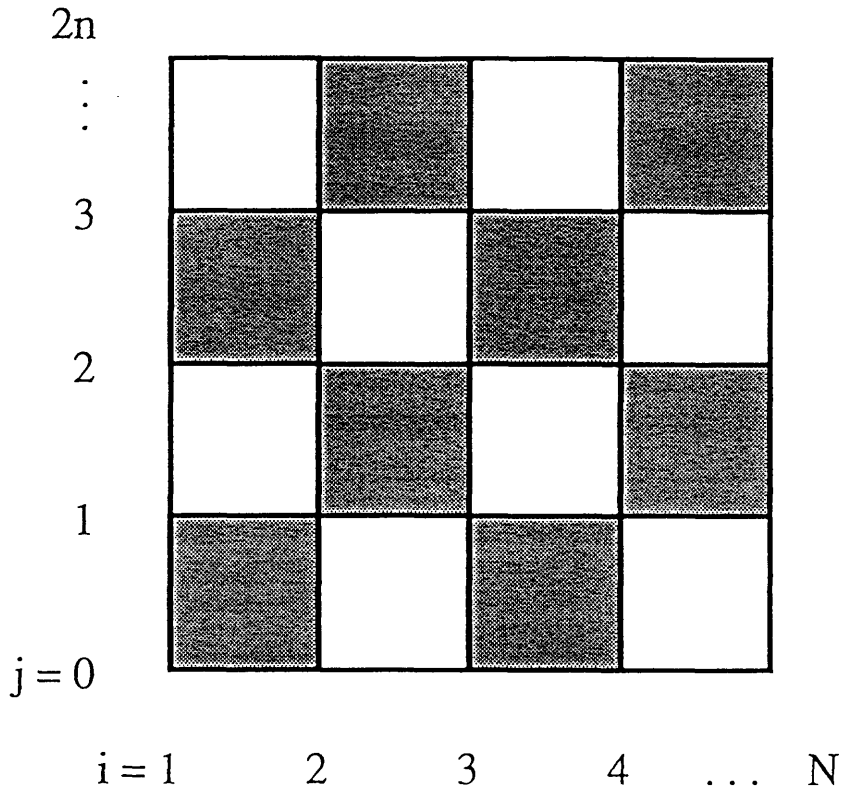

Figure 2-1: The classical $d = 2$ model that is equivalent to the XXZ Heisenberg quantum-spin chain (Ref. [1]). There is a classical variable $m_{i,j} = \pm 1$ at each site (i, j). These are coupled only in the shaded squares, with the interaction of Eq. (2.6), which shows that the model is extremely anisotropic. There are N (the number of the original XXZ Heisenberg spins) sites horizontally and $2n + 1$ (the number of inserted sets of states plus 2) sites vertically. Various specifications of the horizontal boundary conditions determine the property of the original quantum system that is studied via the classical system (Sec. III).

exponentiated Hamiltonian a term

$$e^{-\beta\mathcal{H}_{\square}(m_{i,j},m_{i+1,j},m_{i,j+1},m_{i+1,j+1})} = \begin{bmatrix} A & 0 & 0 & 0 \\ 0 & B & C & 0 \\ 0 & C & B & 0 \\ 0 & 0 & 0 & A \end{bmatrix}$$

$$\text{with } A = e^{K_z/n},\ B = e^{-K_z/n}\cosh(2K/n), \text{ and } C = e^{-K_z/n}\sinh(2K/n), \quad (2.6)$$

where the rows or columns are addressed by the states $(+1,+1)$, $(+1,-1)$, $(-1,+1)$, $(-1,-1)$ of $(m_{i,j}, m_{i+1,j})$ or $(m_{i,j+1}, m_{i+1,j+1})$ respectively. The index i ranges from 1 to N, the number of initial quantum spins, and the index j ranges from 0 to $2n$, the number of inserted sets of kets plus the two states of the matrix element of Eq. (2.5). The expression in Eq. (2.6) is the direct result of the local calculation, described in the preceding paragraph, of

$$\langle m_{i,j}, m_{i+1,j}| \exp\left[(K/n)(\sigma_i^x\sigma_{i+1}^x + \sigma_i^y\sigma_{i+1}^y) + (K_z/n)\sigma_i^z\sigma_{i+1}^z\right] |m_{i,j+1}, m_{i+1,j+1}\rangle, \quad (2.7)$$

where $m_{i,j}$ is the eigenvalue of σ_i^z in the inserted set j. The above clearly corresponds to a classical spin-$\frac{1}{2}$ Ising model, with local constraints, namely excluded nearest-neighbor quartets of states, due to the zeroes in the matrix in Eq. (2.6).

III. Boundary Conditions of the Classical Model

A. Corresponding to the partition function of the XXZ model

In Suzuki's original work, the trace of Eq. (2.5) is taken, in order to obtain the partition function of the XXZ Heisenberg model. This yields the partition function of the equivalent classical $d = 2$ model with periodic boundary conditions along the j direction as defined in Eq. (2.6), $m_{i,0} \equiv m_{i,2n}$. The boundary condition along the i direction is always determined by that of the XXZ model, which we take as periodic in the entirety of this article. Furthermore, N is taken to be large (approaching the thermodynamic limit) and even.

B. Corresponding to the z-aligned state of the XXZ model

The diagonal matrix element of Eq. (2.5) with respect to the quantum state $|\{m_i = +1\}\rangle$ yields, in the classical $d = 2$ model, the pinned "up" boundary conditions $m_{i,0} = +1 = m_{i,2n}$. The constraints [Eq. (2.6)] do not allow the creation of a "down" spin ($m_{i,j} = -1$), so that only one state, $\{m_{i,j} = +1\}$, occurs in the classical system. Thus,

$$\begin{aligned} \langle\{m_i = +1\}|e^{-\beta\mathcal{H}_{XXZ}}|\{m_i = +1\}\rangle &= e^{-\beta\Sigma\mathcal{H}_{\square}(+1,+1,+1,+1)} \\ &= A^{Nn} = e^{NK_z}. \end{aligned} \tag{2.8}$$

The energy of the z-aligned state, NK_z, is the ground-state energy of the XXZ model for $K_z > |K|$ and $K_z = K$.

C. Corresponding to a single spin wave

Consider the matrix element of Eq. (2.5) between states such as $|\{m_{i\neq r} = +1\}, m_{i=r} = -1\rangle \equiv |r\rangle$. This yields the partition function of the classical $d = 2$ model with pinned up boundary conditions at rows $j = 0$ and $j = 2n$, except for the spins at $i = r_0$ and $i = r_{2n}$, respectively, which are pinned down. Since the constraints [Eq. (2.6)] do not allow the creation or destruction of a down spin, each row j has one and only one down spin, which, from row to row, may remain at the same position r, or move to $r \pm 1$ with an interaction square, respectively, with Boltzmann weight B or C according to the interations in Eq. (2.6). Consider the transfer matrix of the classical system, connecting every other row, with respect to the single spin-wave basis set

$$|k\rangle = \frac{1}{\sqrt{N}} \sum_r e^{ikr}|r\rangle, \; k = 2\pi p/N, \; p = 1, \ldots, N. \tag{2.9}$$

A little algebra starting from Eq. (2.6) yields, for this transfer matrix, to leading order in $1/n$,

$$\langle k'|e^{-\beta\mathcal{H}_1/n}e^{-\beta\mathcal{H}_2/n}|k\rangle = \delta(k',k)e^{[NK_z-4K_z+4K\cos k]/n}, \tag{2.10}$$

where $\delta(k',k) = 1,0$ for $k' = k$, $k' \neq k$. Thus, the partition function of the entire system (of n pairs of rows) is

$$\langle k'|(e^{-\beta\mathcal{H}_1/n}e^{-\beta\mathcal{H}_2/n})^n|k\rangle = \delta(k',k)e^{NK_z-4K_z+4K\cos k}, \tag{2.11}$$

which yields the well-known single spin-wave energy

$$\beta\varepsilon_1 = -4K_z + 4K\cos k. \tag{2.12}$$

D. Corresponding to two spin waves

Consider the matrix element of Eq. (2.5) between the states such as $|\{m_{i\neq r,r'} = +1\}, m_{i=r,r'} = -1\rangle \equiv |r,r'\rangle$. This yields the partition function of the classical $d = 2$ model with pinned up boundary conditions at rows $j = 0$ and $j = 2n$, except for the spins at $i = r_0, r_0'$ and $i = r_{2n}, r_{2n}'$, respectively, which are pinned down. Similarly to the previous case, each row j has two and only two down spins, which from row to row, may remain at the same positions r, r', or each or both move to neighboring positions within an interaction square, with Boltzmann weights dictated by Eq. (2.6). Again consider the transfer matrix of the classical system, connecting every other row,

$$\frac{1}{2}\{\langle r_1', r_2'|e^{-\beta\mathcal{H}_1/n}e^{-\beta\mathcal{H}_2/n}|r_1, r_2\rangle + \langle r_1', r_2'|e^{-\beta\mathcal{H}_1/n}e^{-\beta\mathcal{H}_2/n}|r_2, r_1\rangle\}. \tag{2.13}$$

There are two terms in Eq. (2.13) because, in going between the rows, either down spin can match to a give down spin in the other row. There is a leading factor of $\frac{1}{2}$ because the down spins are indistinguishable, so that a summation over (r_1, r_2)

double counts the states. With respect to another two-spin-wave basis set,

$$|k,\rho\rangle = \frac{1}{\sqrt{N}}\sum_{r_1} e^{ik(r_1+r_2)/2}|r_1, r_2 = r_1+\rho\rangle,\ k = 2\pi p/N,\ p = 1,\ldots,N. \tag{2.14}$$

This transfer matrix has the form

$$\frac{1}{2}\{\langle k',\rho'|e^{-\beta\mathcal{H}_1/n}e^{-\beta\mathcal{H}_2/n}|k,\rho\rangle + \langle k',\rho'|e^{-\beta\mathcal{H}_1/n}e^{-\beta\mathcal{H}_2/n}|k,-\rho\rangle\}. \tag{2.15}$$

It reduces to leading order in $1/n$ to

$$\frac{1}{2}\delta(k',k)A^{N-4}[M(\rho',\rho) + e^{ikN/2}M(\rho',N-\rho)], \tag{2.16}$$

where

$$M(\rho',\rho) = \begin{bmatrix} 1 & \gamma & & & & \\ \gamma & 1-\alpha & \gamma & & & \\ & \gamma & 1-\alpha & \gamma & & \\ & & & \cdots & & \\ & & & & \gamma & 1 \end{bmatrix},$$

with

$$\alpha = 4K_z/n,\ \gamma = (4K/n)\cos(k/2),$$

and where ρ',ρ are between 1 and $N-1$ inclusive. The eigenvectors of this tranfer matrix have the form

$$Y(\rho) = x^\rho + bx^{N-\rho},\ \text{with } b = e^{-ikN/2} = \pm 1. \tag{2.17}$$

One set of eigensolutions are extended (unbound) spin-wave pair states with $x = e^{iq}$ in Eq. (2.17). Their eigenvalues are

$$e^{[(N-8)K_z + 8K\cos(k/2)\cos q]/n}, \tag{2.18}$$

where, as specified above, $k = 2\pi p/N$, $p = 1, \ldots, N$, and q is determined for $b = +1$ by

$$(K/K_z)\cos(k/2) - \cos q = \sin q \tan(Nq/2), \tag{2.19}$$

and for $b = -1$ by

$$(K/K_z)\cos(k/2) - \cos q = -\sin q \cot(Nq/2). \tag{2.20}$$

For $|(K/K_z)\cos(k/2)| \geq 1$, graphical analysis shows that Eq. (2.19) accounts for $(N/2)(N/2)$ solutions and Eq. (2.20) accounts for $(N/2)[(N/2) - 1]$ solutions. For $|(K/K_z)\cos(k/2)| < 1$, again graphical analysis shows that Eq. (2.19) accounts for $(N/2)[(N/2) - 1]$ solutions and Eq. (2.20) accounts for $(N/2)[(N/2) - 2]$ solutions. In the latter case, a set of N eigensolutions of bound spin-wave pair states occurs, with $x = |(K/K_z)\cos(k/2)|$ in Eq. (2.17), and eigenvalue

$$e^{\{(N-4)K_z + 4[K\cos(k/2)]^2/K_z\}/n}. \tag{2.21}$$

The expressions in (2.18) and (2.21), with their exponents multiplied by n, yield the corresponding Boltmann weights of the entire system. Thus, the extended spin-wave pair energies are

$$\begin{aligned} -\beta\epsilon_2 &= -8K_z + 8K\cos(k/2)\cos q \\ &= -8K_z + 4K[\cos(k/2 + q) + \cos(k/2 - q)], \end{aligned} \tag{2.22}$$

which in fact equals the sum of the energies [Eq. (2.12)] of two single spin waves with wave numbers $(k/2) \pm q$. The bound spin-wave pair states, occurring for $|(K/K_z)\cos(k/2)| < 1$ as above, have energy

$$-\beta\varepsilon_2 = -4K_z + 4[K\cos(k/2)]^2/K_z. \tag{2.23}$$

The above account for all of the spin-wave pair states, and agree with the previous works [7, 8, 9, 10].

A particulate analogy to two interacting spin waves, from the diagonalization of the matrix in Eq. (2.16), is given in Appendix A. A renormalization-group transformation is derived in Appendix B, with asymptotic flow behavior that is fixed point or chaotic, distinguishing the bound or extended spin-wave pairs, respectively.

E. Corresponding to three spin waves

The matrix element of Eq. (2.5) between the states such as $|\{m_{i\neq r,r',r''}=+1\},m_{i=r,r',r''}=-1\rangle$ is considered. The classical $d=2$ model has pinned up boundary conditions at rows $j=0$ and $j=2n$, except for the spins at $i=r_0,r_0',r_0''$ and $i=r_{2n},r_{2n}',r_{2n}''$, respectively, which are pinned down. Each row j has three and only three down spins, which from row to row, may remain at the same positions r,r',r'', or move to neighboring positions within an interaction square, with Boltzmann weights dictated by Eq. (2.6). The transfer matrix of the classical system, connecting every other row, with respect to the three-spin-wave basis set

$$|k,\rho_1,\rho_3\rangle=\frac{1}{\sqrt{N}}\sum_{r_2}e^{ik(r_1+r_2+r_3)/3}|r_1=r_2-\rho_1,r_2,r_3=r_2+\rho_3\rangle,$$

$$\text{with } k=2\pi p/N,\ \ p=1,\ldots,N,\ \ \rho_1=1,\ldots,N-2,$$

$$\text{and } \rho_3=1,\ldots,N-1-\rho_1, \tag{2.24}$$

has the form

$$\tfrac{1}{3}\{\langle k',\rho_1',\rho_3'|e^{-\beta\mathcal{H}_1/n}e^{-\beta\mathcal{H}_2/n}|k,\rho_1,\rho_3\rangle+\langle k',\rho_1',\rho_3'|e^{-\beta\mathcal{H}_1/n}e^{-\beta\mathcal{H}_2/n}|k,-\rho_1-\rho_3,\rho_1\rangle$$

$$+\langle k',\rho_1',\rho_3'|e^{-\beta\mathcal{H}_1/n}e^{-\beta\mathcal{H}_2/n}|k,\rho_3,-\rho_1-\rho_3\rangle\}. \tag{2.25}$$

Again, there are three terms in Eq. (2.25) because, in going between the rows, any one of the three down spins can match to a given down spin in the other row (which fixes the other two matches). There is a leading factor of $\frac{1}{3}$ because the down spins are indistinguishable, so that a summation over (ρ_1, r_2, ρ_3) triple counts the states. The first term in the parentheses of Eq. (2.25), for exmaple, reduces to leading order in $1/n$ to

$$\begin{aligned}\delta(k',k)A^{N-6}B^6\Big(&\delta(\rho_1',\rho_1)\delta(\rho_3',\rho_3)\Big\{1+\alpha[\delta(\rho_1,1)+\delta(\rho_3,1)+\delta(\rho_1+\rho_3,N-1)]\Big\}\\ &+C\Big\{[e^{ik/3}\delta(\rho_1',\rho_1-1)+e^{-ik/3}\delta(\rho_1',\rho_1+1)]\delta(\rho_3',\rho_3)\\ &+\delta(\rho_1',\rho_1)[e^{-ik/3}\delta(\rho_3',\rho_3-1)+e^{ik/3}\delta(\rho_3',\rho_3+1)]\\ &+e^{ik/3}\delta(\rho_1',\rho_1+1)\delta(\rho_3',\rho_3-1)+e^{-ik/3}\delta(\rho_1',\rho_1-1)\delta(\rho_3',\rho_3+1)\Big\}\Big). \qquad (2.26)\end{aligned}$$

The transfer matrix of Eq. (2.25) has a set of bound-state eigenvectors of the form

$$Y(\rho_1,\rho_3)=y(\rho_1,\rho_3)+by(N-\rho_1-\rho_3,\rho_1)+b^2y(\rho_3,N-\rho_1-\rho_3), \qquad (2.27)$$

with

$$\begin{aligned} b &= e^{-iNk/3},\\ y(\rho_1,\rho_3) &= e^{-i\phi(\rho_1-\rho_3)}x^{\rho_1+\rho_3},\\ \sin(k/3+\phi) &= \sin k/\sqrt{1+4(K_z/K)\cos(k)+4(K_z/K)^2}, \end{aligned}$$

where the spatial decay is determined by

$$x=\sin(k/3+\phi)/\sin(k/3-2\phi),\ |x|<1, \qquad (2.28)$$

where the bound-state restriction $|x|<1$ is satisfied for $(K/K_z)\cos k < [4(K_z/K)^2-3]$. The corresponding eigenvalues are

$$\begin{aligned}&\exp\{[(N-4)K_z+4Kx\cos(k/3+\phi)]/n\}\\ &=\exp\{[(N-4)K_z+4K^2(2K_z+K\cos k)/(4K_z^2-K^2)]/n\}. \qquad (2.29)\end{aligned}$$

Thus, the corresponding three-spin-wave bound-state energies are

$$\begin{aligned} -\beta\varepsilon_3 &= -4K_z + 4Kx\cos(k/3+\phi) \\ &= -4K_z + 4K^2(2K_z + K\cos k)/(4K_z^2 - K^2). \end{aligned} \tag{2.30}$$

These bound-state energies are depicted in Fig. 2-2. The particulate analogy to three interacting spin waves, from the diagonalization of the matrix in Eq. (2.26), is noted in Appendix A.

IV. Conclusion

As seen above, the continuum energetics of the elementary excitations of a d-dimensional quantum model are contained in the equivalent $(d+1)$-dimensional classical model, even though the latter is a discrete-spin model. This is due to the fact that the extreme anisotropy of the classical model reduces the problem to a diagonalization of the Hamiltonian, as $n \to \infty$. In this process, we have derived three-spin-wave bound-state energies for the XXZ Heisenberg chain.

The implementation of our method is rather different from Bethe ansatz [7] studies of quantum systems. The method can also be generalized to, for example, spin-s systems. Our method is also much simpler, and therefore much more transparent, than the "quantum inverse scattering method." [11]

The procedure introduced here of using the Suzuki-Trotter formula with restricted boundary conditions may be useful for obtaining "renormalized" or "dressed" energy spectra for elementary excitations in more difficult problems, such as ones in which the transfer matrix does not conserve the number of fluctuations. More generally, it is likely that diverse effective studies of quantum systems can be built around the Suzuki-Trotter mapping.

Acknowledgements

This research was supported by the U.S. Department of Energy under Grant No. DE-FG02-92ER45473. D.P.A. acknowledges partial support from the NSF during

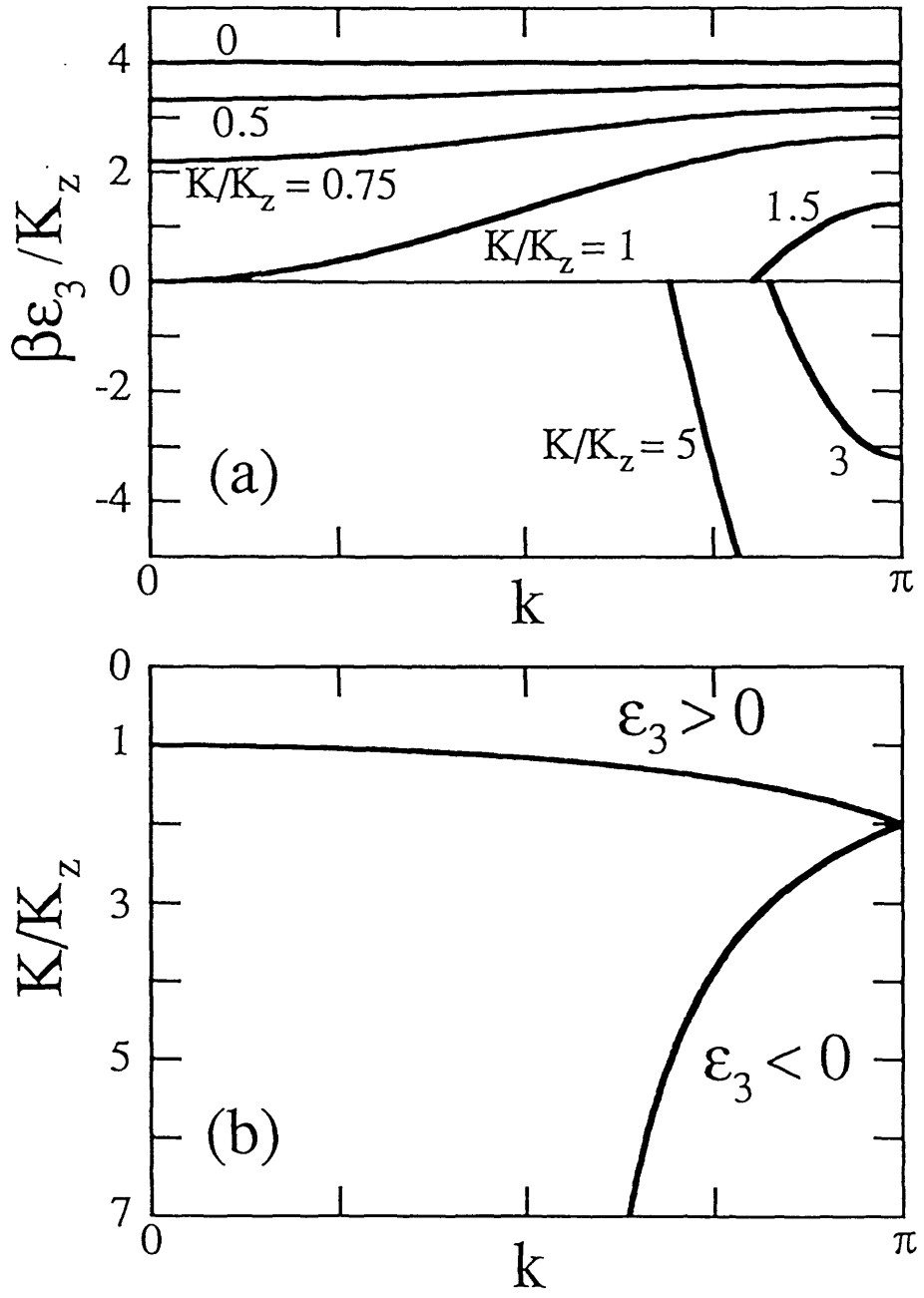

Figure 2-2: (a) Bound-state energy spectra for three spin waves, as derived in Sec. III E and given in Eq. (2.27). Bound-state energy spectra for $K/K_z < 0$ or $k < 0$ are related to these curves by $\varepsilon_3(K/K_z, k) = \varepsilon_3(-K/K_z, k+\pi) = \varepsilon_3(K/K_z, -k)$. (b) Regions in which the three-spin-wave bound states with energies given in Eq. (2.30) occur. The lower boundary reaches $k = \pi/2$ as K/K_z goes to infinity.

the initial stage of this research.

Appendix A: Particulate Analogy to Interacting Spin Waves

The matrix in Eq. (2.16) can be written as

$$M(\rho',\rho) = \{\gamma\Delta^2 + \alpha[\delta(\rho,1) + \delta(\rho,N-1)] + (1-\alpha+2\gamma)\}\delta(\rho',\rho), \tag{2.31}$$

where Δ^2 is the discrete Laplacian operator,

$$\Delta^2 Y(\rho') = Y(\rho'+1) - 2Y(\rho') + Y(\rho'-1). \tag{2.32}$$

Accordingly, diagonalizing M is equivalent to solving the one-dimensional discrete Schrödinger equation for a particle of mass m in an infinite well from $\rho = 1$ to $\rho = N-1$, subject to a potential at the edge sites, namely

$$V(\rho) = -\hbar^2/|2m(K/K_z)\cos(k/2)|[\delta(\rho,1) + \delta(\rho,N-1)]. \tag{2.33}$$

The absolute value is obtained by considering the vectors $(-1)^\rho Y(\rho)$ when $(K/K_z)\cos(k/2) < 0$. The particle of this Schrödinger equation may have eigenstates bound to the edges. The condition for this turns out to be $|(K/K_z)\cos(k/2)| < 1$. The combination of two matrices in Eq. (2.16) selects half of the even and odd eigenfunctions of M, for both bound and extended states.

Simlarly, the three-spin-wave problem of Sec. III E is equivalent to the two-dimensional discrete Schrödinger equation for a particle in an equilateral-triangle infinite well, with a potential along the sides that doubles at the corners.

Appendix B: Renormalization-Group Analysis of the Two-Spin-Wave Eigenvalue Problem

The eigenvalue Λ problem for the matrix M in Eq. (2.16) reduces to the $N-1$ equations

$$Fx_1 + x_2 = 0, \;\; x_{\rho-1} + Gx_\rho + x_{\rho+1} = 0 \text{ for } \rho = 2 \text{ to } N-2,$$
$$x_{N-2} + Fx_{N-1} = 0, \tag{2.34}$$

where

$$F = (1-\Lambda)/\gamma \;\text{ and }\; G = (1-\alpha-\Lambda)/\gamma. \tag{2.35}$$

A renormalization-group recursion [12] can be constructed by substituting every other equation into the remaining ones, resulting in $N/2$ equations of the same form, but with renormalized coefficients:

$$F' = 1 - FG \;\text{ and }\; G' = 2 - G^2. \tag{2.36}$$

The procedure is repeated, but with one of the edge coefficients having its recursion modified as

$$F' = 1 - G^2 + G/F, \tag{2.37}$$

if the starting number of equations is even, in which case this number is halved. In any case, the recursion of the inner coefficient G depends only on itself. It has unstable fixed points at $G^* = 1$ and -2, with a preimage of the latter at $G = 2$. This recursion remains chaotic in the interval $|G| < 2$, and runs away to the fixed point $G^* = -\infty$ and $F^* = -\infty$ for $|G| > 2$. The extended and bound states found in Sec. III D, in fact, respectively fall into the chaotic and runaway fixed-point renormalization-group behaviors. In previous works on electronic [13] and harmonic [14] chains, it was similarly found that extended and localized states, respectively, have chaotic and fixed-point renormalization-group behaviors [15].

References

[1] M. Suzuki, Prog. Theor. Phys. **56**, 1454 (1976).

[2] H.F. Trotter, Proc. Am. Math. Soc. **10**, 545 (1959).

[3] M. Suzuki, S. Miyashita, and A. Kuroda, Prog. Theor. Phys. **58**, 1377 (1977).

[4] *Quantum Monte Carlo Methods in Equilibrium and Non-Equilibrium Systems*, edited by M. Suzuki (Springer, Berlin, 1987).

[5] H.-Q. Ding and M.S. Makivić, Phys. Rev. Lett. **46**, 1449 (1990).

[6] M.S. Makivić, Phys. Rev. B **46**, 3167 (1992).

[7] H. Bethe, Z. Phys. **71**, 205 (1931).

[8] F. Dyson, Phys. Rev. **102**, 1217 (1956); **102**, 1230 (1956).

[9] R. Orback, Phys. Rev. **112**, 309 (1958).

[10] M. Wortis, Phys. Rev. **132**, 85 (1963).

[11] Yu.A. Izyumov and Yu.N. Skryabin, *Statistical Mechanics of Magnetically Ordered Systems* (Plenum, New York, 1988), Chap. 5. This approach builds on Baxter's results of relating the XYZ Hamiltonian to the eight-vertex model [R.J. Baxter, *Exactly Solved Models in Statistical Mechanics* (Acedemic, London, 1982)].

[12] Renormalization-group studies of the two-spin-wave problem, for spin-s chains, are in B.W. Southern, T.S. Liu, and D.A. Lavis, Phys. Rev. B **39**, 12160 (1989); S.C. Bell, P.D. Loly, and B.W. Southern, J. Phys. Condens. Matter **1**, 9899 (1989); A.J.M. Medved, B.W. Southern and D.A. Lavis, Phys. Rev. B **43**, 816 (1991).

[13] B.W. Southern, A.A. Kumar, P.D. Loly, and A.-M.S. Tremblay, Phys. Rev. B **27**, 1405 (1983).

[14] J.-M. Langois, A.-M.S. Tremblay, and B.W. Southern, Phys. Rev. B **28**, 218 (1983).

[15] A previous example of chaotic renormalization-group trajectories is in spin glasses, where the coupling strengths of the system rescale chaotically. See S.R. McKay, A.N. Berker, and S. Kirkpatrick, Phys. Rev. Lett. **48** 767 (1982).

2.2 Quantum XY-Model

The model Hamiltonian for the classical XY model in two dimensions is

$$-\beta\mathcal{H} = K\sum_{\langle ij\rangle}\cos(\theta_i - \theta_j), \tag{2.38}$$

where $\langle ij\rangle$ denotes nearest neighbors i and j and θ_i is the angle describing the vector at site i. Equation (2.38) represents systems from two-dimensional superfluids to liquid crystals.

Low temperature expansion of the Hamiltonian yields a gaussian model:

$$-\beta\mathcal{H} \approx K\sum_{\langle ij\rangle}\left[1-(\theta_i-\theta_j)^2/2\right]. \tag{2.39}$$

Fluctuations drive long-wavelength spin waves such that misalignment grows logarithmically with distance and long range order is destroyed. Mermin and Wagner[2] proved rigorously that there can be no long range order — *i.e.* $M = 0$ even in the low temperature phase — for the XY model in two dimensions. Nevertheless, Stanley[3] showed using high-temperature series expansion that the susceptibility diverged to indicate a finite-temperature critical point.

Kosterlitz and Thouless[4] realized that there was the possibility for other types of excitations which could appear in addition to the slow variations of θ observed in the Gaussian model. These excitations are topological defects called vortices. A vortex pair is depicted in Fig. 2-3.

Vortices arise from the fact that the cosine function that defines the original model is periodic. Following the angle around a defect counterclockwise leads to a change of phase equal to an integer multiple of 2π:

$$\theta \rightarrow \theta + 2\pi Q. \tag{2.40}$$

[2]N.D. Mermin and H. Wagner, Phys. Rev. Lett. **17**, 1133 (1967).

[3]H.E. Stanley, Phys. Rev. Lett. **20**, 150 (1968).

[4]J.M. Kosterlitz and D.J. Thouless, J. Phys. C **6**, 1181 (1973); J.M. Kosterlitz, J. Phys. C **7**, 1046 (1974).

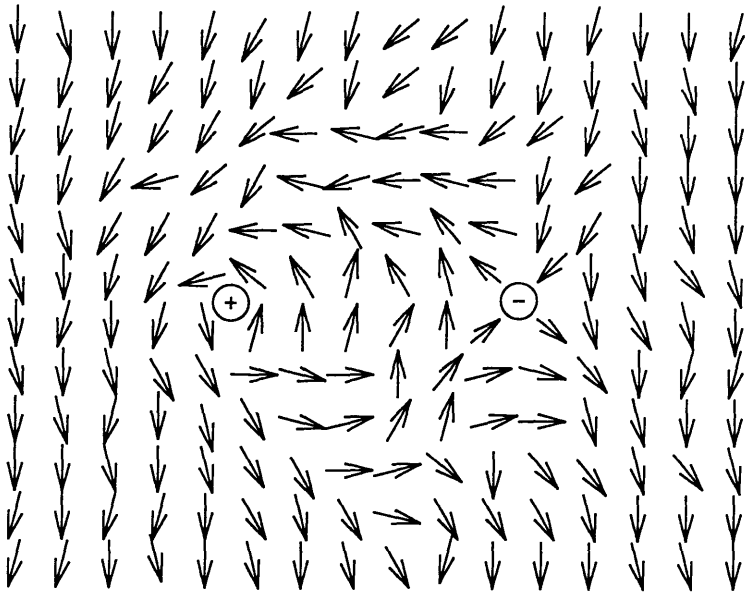

Figure 2-3: A vortex pair in the classical model. The vectors point in the direction characterized by θ. The "charges" Q [defined in Eq. (2.40)] are determined by measuring the change in the angle if one follows a closed path counterclockwise around the vortex. Note that θ is unaffected far away from a vortex pair.

One can calculate the energy, entropy, and free energy of a lone vortex:

$$-\beta E = 2\pi K \ln(L/a), \tag{2.41}$$

$$\beta T S = \ln (L/a)^2 , \tag{2.42}$$

$$-\beta F = -\beta(E - TS) = (-2\pi K + 2)\ln(L/a). \tag{2.43}$$

The system is unstable to the formation of single vortices at temperature high enough such that $K < K_c = \pi^{-1}$.

At low temperatures vortices could appear in pairs (a $+1$ vortex with a -1 vortex) with a non-divergent energy since the defects neutralize each other and far away $Q_{\rm net} = 0$. Pairs of vortices are also found to unbind at $K = K_c$.

Kosterlitz and Thouless description for what happens at the phase transition appeals strongly to intuition. For high temperatures, there is a free gas of vortices which bind into pairs below the K_c.

Renormalization-group treatments of interacting vortices were carried out by sev-

eral groups.[5]

The two-dimensional XY model is peculiar because the low temperature phase is not an ordered phase, in the conventional sense. Its onset is also unlike most other phase transitions because instead of power law divergences at the critical point (as discussed in Ch. 1),

$$M \sim \left(\frac{T_c - T}{T_c}\right)^{\beta},$$

quantities like the correlation length ξ in the XY model diverge with an exponential dependence as the critical temperature is approached from above,

$$\xi \sim \exp\{A/\sqrt{T - T_c}\}, \tag{2.44}$$

where A is a constant.

In the following article, "Entanglement Transition in the Two-Dimensional Quantum XY Model," I examine the quantum mechanical analog of Eq. (2.38). I propose an intuitive picture which readily distinguishes the high and low temperature phases and allows for direct quantitative analysis. This published work may be found in Phys. Rev. B **49**, 7040 (1994).

[5]J.M. Kosterlitz, J. Phys. C **7**, 1046 (1974); J.V. José, L.P. Kadanoff, S. Kirkpatrick, and D.R. Nelson, Phys. Rev. B **16**, 1217 (1977); A.N. Berker and D.R. Nelson, Phys. Rev. B **19**, 2488 (1979).

Entanglement Transition in the Two-Dimensional Quantum XY Model

Daniel P. Aalberts

Department of Physics, Massachusetts Institute of Technology, Cambridge, Massachusetts 02139

Abstract

We use the Suzuki-Trotter transformation to map exactly the fully quantum mechanical XY model in 2-dimensions to a classical system in $(2+1)$-dimensions. In the latter formulation the phase transition is intuitively described and order parameters are introduced. A Monte Carlo study confirms this picture's transition takes the Kosterlitz-Thouless form. Two additional local symmetries which have, to date, been neglected in Quantum Monte Carlo simulations, are revealed and used.

PACS Numbers 75.10.Jm, 75.40.Mg, 05.70.Fh, 64.60.Cn

The $d = 2$ spin-$\frac{1}{2}$ XY model has been extensively studied because it is the simplest unsolved model incorporating non-commuting operators. It is defined by

$$-\beta H = K \sum_{\langle ij \rangle} (\sigma_i^x \sigma_j^x + \sigma_i^y \sigma_j^y), \tag{2.45}$$

where $\beta^{-1} = kT$, $\langle ij \rangle$ denotes nearest neighbors, and σ are the spin-$\frac{1}{2}$ Pauli operators. In the classical (vector) equivalent of Eq. (2.45), Kosterlitz and Thouless [1] showed how the binding and unbinding of pairs of topological defects called vortices lead to a transition to a low-temperature phase with infinite correlation length but no long-range order. One may question whether quantum fluctuations might change the form of this marginal transition or destroy it altogether.

Several techniques have been used on the spin-$\frac{1}{2}$ problem. A high-temperature series [2] indicated a finite critical temperature and a divergent susceptibility but was unable to determine whether the transition took the Kosterlitz-Thouless (KT) form. Work [3] was carried out by neglecting commutator terms arising in the Boltzmann weight, which indicated a divergence in the specific heat of the system. The Suzuki-Trotter (ST) transformation [4], which maps a d-dimensional quantum system to a $(d+1)$-dimensional system with classical variables, has primarily enabled Monte Carlo (MC) simulations.[5] MC studies examined quantum vortex operators or calculated susceptabilities or correlation functions [6, 7, 8, 9]. Recent MC results indicate that although quantum fluctuations suppress the transition temperature, the KT transition remains [9].

One difficulty common to all of these techinques is that one cannot visualize the problem as one can with, say, vector representations of classical spins. This is a general problem in quantum statistical mechanics which the ST mapping may alleviate. Curiously, describing what happens when the temperature is lowered in the ST representation of the $d = 2$ spin-$\frac{1}{2}$ XY model is as simple as visualizing a pot of spaghetti cooking: the strands begin as rigid poles but as they soften they begin to tangle until they wind around one another. Our approach will be to take the ST transformation at face value to formulate a picture of the transition in the (2+1)-

dimensional system, quantify by inventing order parameters, and then verify with a MC study. The critical temperature $T_c = 1.50 \pm 0.03$ is inferred from the scaling behavior of these quantities. Also, while preparing the MC calculation, additional local symmetry operations are discovered.

The partition function is calculated using the Trotter [10] transformation popularized by Suzuki. The ST identity [4] is

$$\begin{aligned} Z &= \mathrm{Tr}\{e^{-\beta H}\} = \mathrm{Tr}\{e^{-\beta(H_1+H_2+H_3+H_4)}\}, \\ Z &= \lim_{n\to\infty} \mathrm{Tr}\{(e^{-\beta H_1/n}\cdots e^{-\beta H_4/n})^n\}, \end{aligned} \tag{2.46}$$

where H_μ are sub-Hamiltonians which couple groups of nearest neighbors on a square lattice and where Periodic Boundary Conditions (PBC's) in the spatial directions are used. A complete set of states is inserted between each exponential operator. With the trace yielding periodic boundary conditions in the "Trotter dimension," there are a total of $4n$ interactions, each involving four spins (the shaded squares of Fig. 2-4), stacked above each lattice point. Each of the $4n$ terms in Eq. (2.46) is a product of the nearest-neighbor interactions belonging to the relavent sub-Hamiltonian:

$$\begin{aligned} \langle\{s\}|e^{-\beta H_\mu/n}|\{s'\}\rangle &= \prod_{\langle ij\rangle\in\mu} \Big[\delta(s_i,s_i')\delta(s_j,s_j') \\ &\quad +(2K/n)\delta(s_i,s_j')\delta(s_j,s_i')\delta(s_i,-s_j)\Big], \end{aligned} \tag{2.47}$$

with $s_i = \pm 1$; δ, the Kronecker delta-function; and K, the inverse temperature. Corrections of $O(n^{-2})$ vanish in the large n limit. The magnetization is conserved in the $\hat{z}$ basis representation.

Becuase of the spatial asymmetry of the ST mapping, it is convenient to follow the paths the up spins trace out through the lattice in the Trotter dimension, $\hat{n}$. One can think of these trails as poles (the + spins) which wander in a background of vacancies (the − spins). In the large n limit, Eq. (2.47) says a plus spin is unlikely to hop at any given plaquette; however, with n opportunities there should be $O(K)$ hops per nearest-neighbor pair. That expectation will be modified somewhat because PBC's

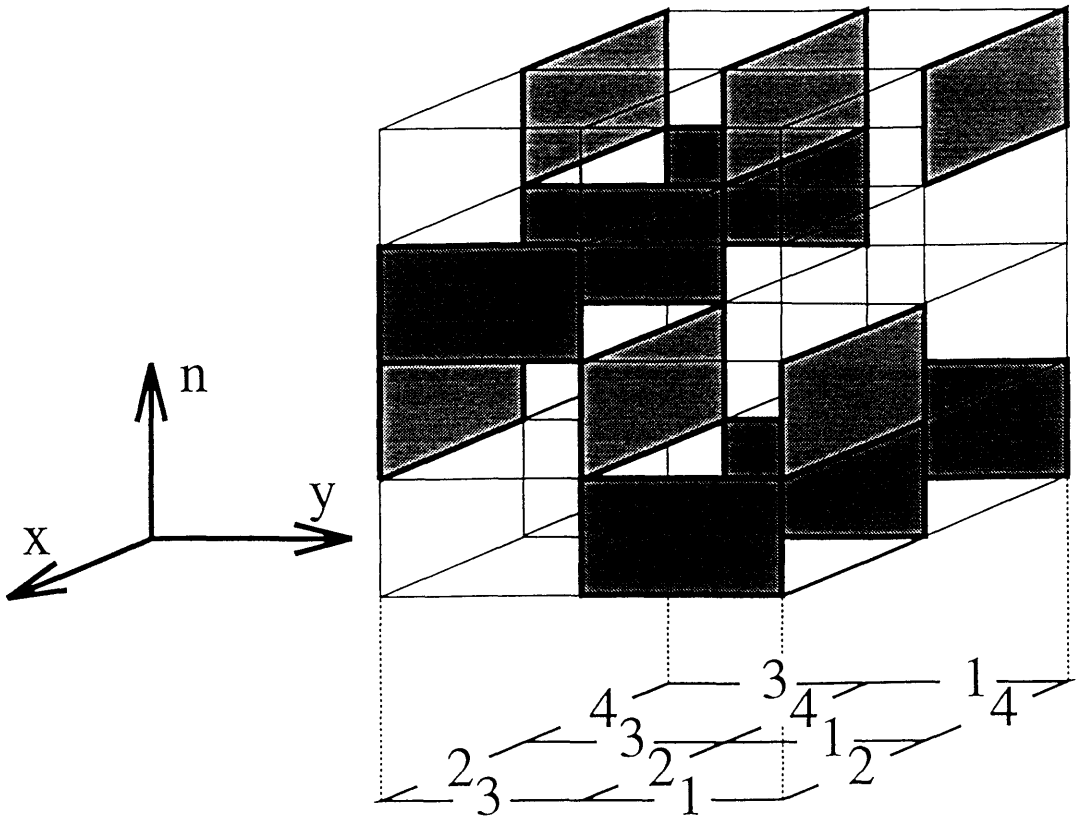

Figure 2-4: The Suzuki-Trotter mapping relates groups of nearest-neighbor quantum couplings in two dimensions ($\widehat{x}$ and $\widehat{y}$ in the figure) to a series of interactions in $(2+1)$ dimensions. Quantum spins are evaluated in a particular basis (yielding Ising spins) and evolve in the additional, "Trotter," dimension, $\widehat{n}$. Each shaded square represents a plaquette interaction which couples two Ising spins at one Trotter height with two Ising spins at the next Trotter height.

in the Trotter dimension require that hops assemble to make loops above the $d = 2$ lattice. "Diagrams" represent connected groups of hops if we imagine looking down the $\hat{n}$ axis.

At infinite temperature, $K = 0$, so the hopping term in Eq. (2.47) is disallowed and the configurations have only poles and vacancies. At high temperatures ($K \ll 1$), most of the poles will not hop [diagram of Fig. 2-5(a)] or will hop to a vacant neighbor and hop-back [Fig. 2-5(b)]. In both cases the pole's PBC in the Trotter direction is met by itself.

At lower temperatures (larger K), another class of excitations begin to contribute. These groups of poles meet PBC's by exchanging positions (twisting, tangling) in the Trotter dimension. "Tangles" are poles which meet each other's PBC's. Entangling diagrams [Figs. 2-5(c)–2-5(e)] involve at least four hops (on a square lattice) and contribute a factor of $(2K)^4/4!$ per diagram to the partition function sum.

Diagrams with a large number of hops pay a large energy price via the partition function factor $(2K)^{N_{\rm hops}}/N_{\rm hops}!$ per ordered, directed diagram; however, the large number of ways of ordering internal to the diagram size ultimately favors larger twisted/entangled diagrams at lower temperatures [11]. This is easily demonstrated by summing the weights, z_ℓ, of all ℓ-site diagrams. To leading order in K: $z_1 = 2$, $z_2 = 8K^2$, $z_3 = 32K^4$, $z_4 = 32K^4$. (Note that z_4 is the first deviation from $z_\ell \sim K^{2(\ell-1)}$.) Figure 2-6 is a diagramatic representation of a configuration obtained in a MC simulation with linear dimension $L = 12$ and with $K = 0.65$.

Work on the "winding number" W provides further insight into the nature of the transition. The winding number measures the net flow of particle lines in the real dimension as paths are followed up the added dimension. Marcu's MC measurement in the spin-$\frac{1}{2}$ XY model [8] and others' work [12] on a system related by universality indicates that at high temperature $\langle |W|^2 \rangle = 0$ with a universal jump to $\langle |W|^2 \rangle \neq 0$ in the low temperature phase. This work indicates, in our language, that tangles extend across the system in the low temperature phase. Tangles woven together (like chain mail) appear in the same diagram. As the temperature decreases to the critical temperature T_c, the largest diagram grows to eventually "percolate" to the

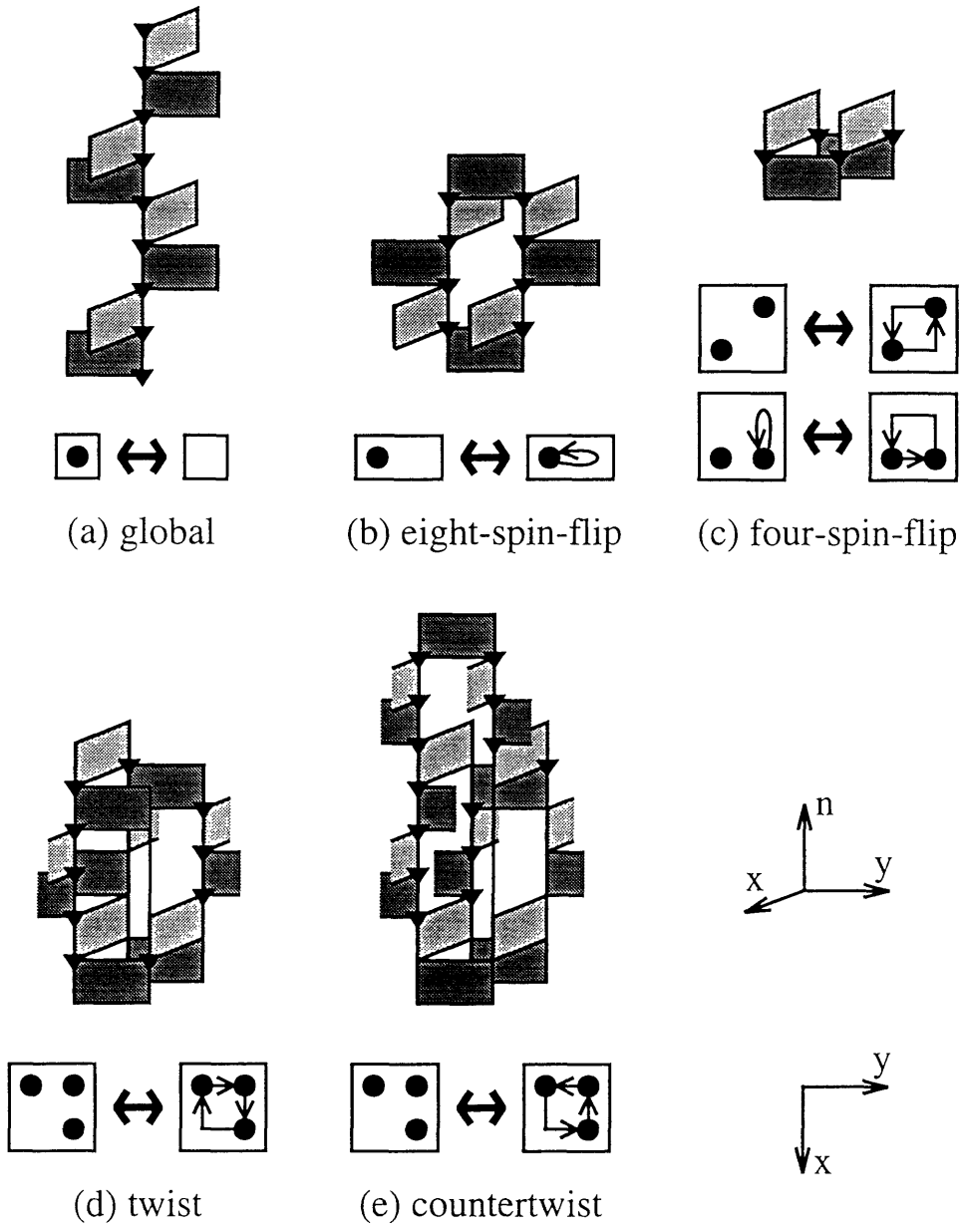

Figure 2-5: Local symmetry operations for MC study: (a)–(c) were used previously; (d)–(e) are introduced here. Dark triangles mark the group of spins in the $(2+1)$-dimensional system which must be simultaneously flipped ($s' = -s$) in a MC trial. In (a), an entire pole of + spins is exchanged for − spins; in (b), by flipping the eight marked spins, a + pole hops across the bottom plaquette and hops back via the top plaquette; in (c), four plaquette hops make two + poles wind around each other. (d) and (e) are operations which wind one + (or −) pole around a loop. If neighbor poles have the same spin, there can be no hopping. Depicted beneath each are examples of diagramatic representations (the paths of + poles above the two-dimensional lattice as seen looking down $\hat{n}$) generated by the operation.

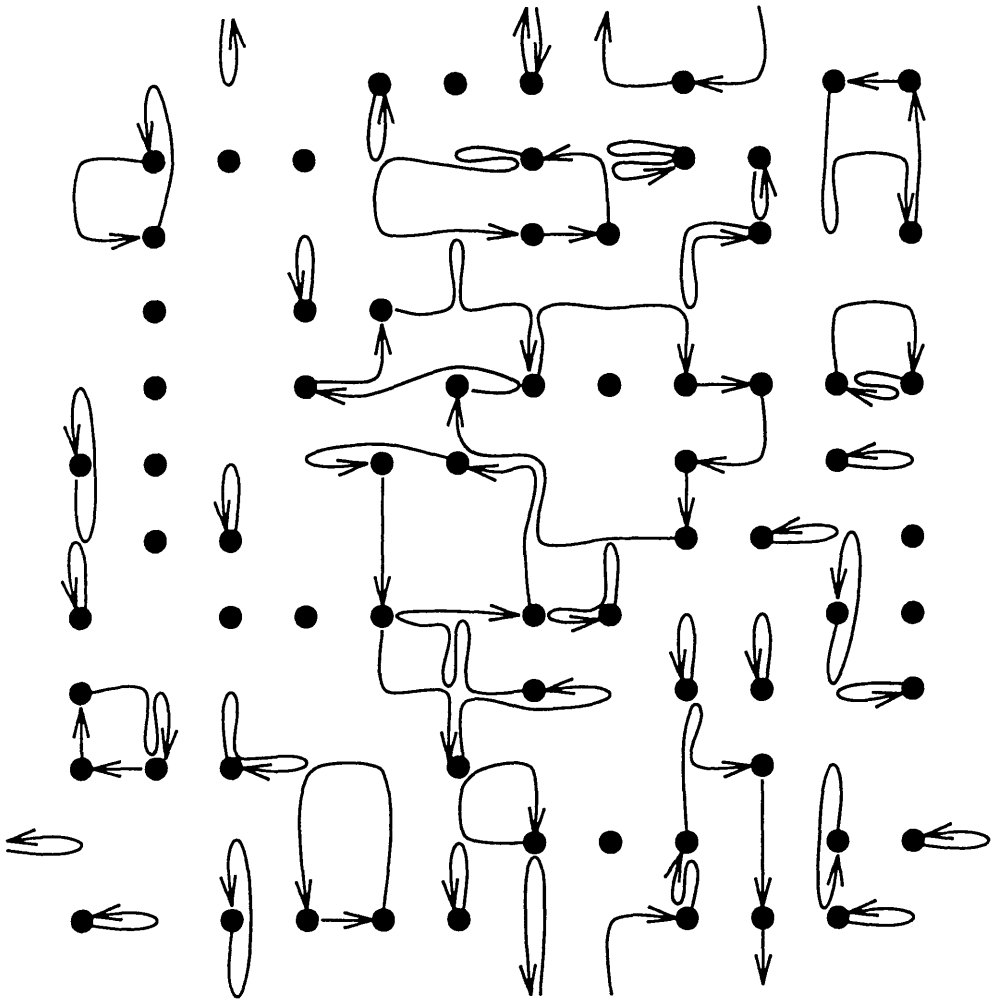

Figure 2-6: Diagrammatic representation of a configuration generated by a Monte Carlo simulation on a 12×12 lattice with periodic boundary conditions at $K = 0.65$. Solid circles represent up spins; arrows, hopping. The largest diagram (connected group of hops) involves 49 sites.

system size. For $T < T_c$, the tangling becomes more complicated and remains infinite. Consistency with the KT picture is suggested by the divergence of the length scales in this formulation, the tangle length and the diagram size.

Now we convert the concepts of tangles and diagrams into calculable quantities. New order parameters are the expectation value for the number of poles contributing to a tangle, τ, and the expectation value of the diagram size, D. To calculate τ, follow a pole in the Trotter direction and count the number of times periodic boundary conditions must be employed before returning to the original lattice point. D is calculated by marking every point which is interconnected by hops, counting the number of points in the diagram, and averaging. A third order parameter, $\langle|\mathbf{r}|^2\rangle$, measures the average deviation squared of the top and the bottom of a pole on the $d = 2$ lattice. Because the number of hops is $O(K)$, $\langle|\mathbf{r}|^2\rangle$ will not diverge at finite K.

MC methods test the qualitative picture described above. Previously used [6, 8, 9, 13] symmetry operations [Figs. 2-5(a)–2-5(c): global-spin-flip, eight-spin-flip, four-spin-flip] neglect some basic diagrams; therefore, we introduce the new symmetry operations shown in Figs. 2-5(d)–2-5(e): twist, and countertwist. Entangling operations [Fig. 2-5(c)–2-5(e)] are introduced only in their most compact (in $\hat{n}$) incarnations. In hopes of better sampling the phase space, the eight-spin-flip is generalized to all length scales by having the hop back take place 1 (the original eight-spin-flip), 2, 4, 8, ..., $2^{p_{n,\max}} < n$ Trotter height unit cells above the hop. The winding number global operation is not used in this simulation.

By calculating dot products of maps of the displacements, $\mathbf{r}$, at different times, we found that correlations fell off with a decay rate of 5 MC steps (MCS) which became our sampling rate. The Trotter number $n = 25$ was chosen to keep errors of fundamental diagrams small.

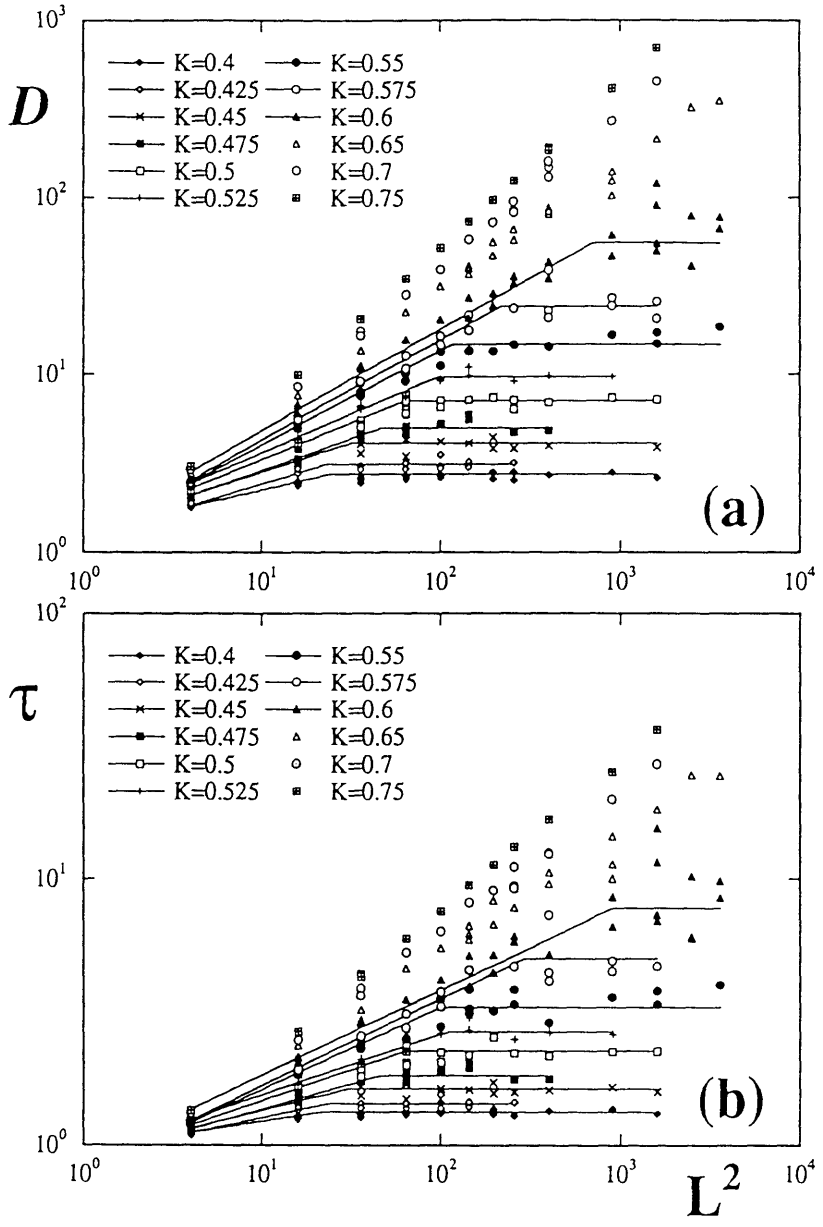

Figure 2-7: (a) D and (b) τ are calculated in our MC study at different coupling constants K and system sizes L^2. Points are typically generated with 5000 MCS, sampling every 5 MCS after discarding 500 MCS.

The results of our MC simulation are displayed in Fig. 2-7. The correlation length ξ can be inferred from the crossover of D and τ from scaling with, to independence from, the system size. The diagram size gives a measure of the average correlated area, so

$$\begin{aligned} D &\sim \int_0^L d^2r\ r^{-\eta} e^{-r/\xi} \\ D &\sim \begin{cases} L^{2-\eta} & , \text{ if } L \ll \xi \\ \xi^{2-\eta} & , \text{ if } L \gg \xi \end{cases} \end{aligned} \tag{2.48}$$

where η is the correlation function critical exponent. So for each temperature, D and τ are fit as powers of L for $L < \xi$ and as constants for $L > \xi$. In this way, ξ is located for each temperature. In Fig. 2-8, the large lattice limit ($L \gg \xi$) for the order parameters (D_∞ and τ_∞), are plotted alongside the correlation lengths derived from D and τ (ξ_D and ξ_τ). A critical temperature, $T_c = 1.50 \pm 0.03$, is obtained from fitting all of these quantities to the KT form divergence

$$C \exp\{A/\sqrt{T - T_c}\}, \tag{2.49}$$

where A and C are constants.

A correlation function is needed to study short-range correlations and to calculate $\eta(T)$ for $T < T_c$. We propose that x-y correlation can be measured by considering points within the same diagram correlated and points in different diagrams uncorrelated.

Large lattice, large Trotter number simulations should be run to study nearer T_c.

I thank A. Nihat Berker for helpful comments and for suggesting the problem. This work was supported by the U.S. Department of Energy under Grant No. DE-FG02-92ER45473.

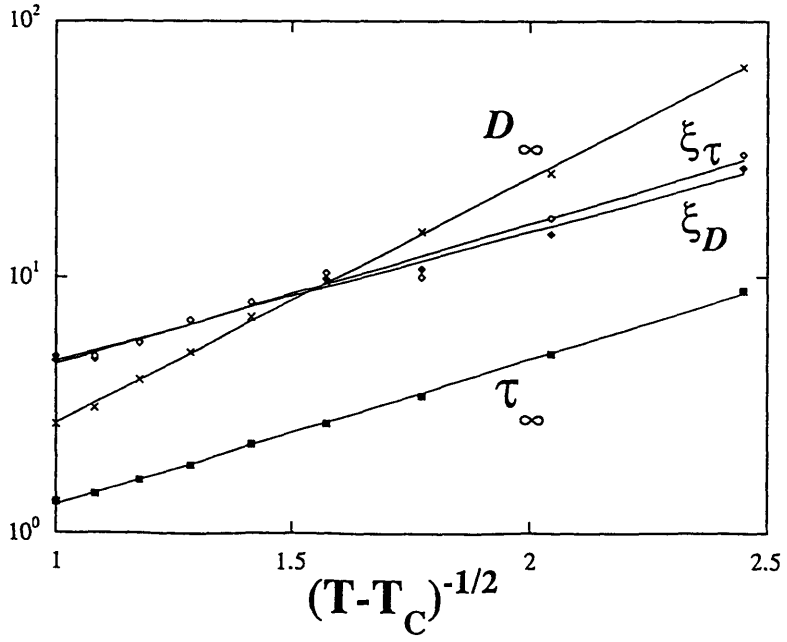

Figure 2-8: Correlation lengths (ξ_D and ξ_τ) and the large lattice limits (D_∞ and τ_∞) calculated from Fig. 2-7(a,b) are fit to the KT form [Eq. (2.49)]. $T_c = 1.5$ is used.

References

[1] J.M. Kosterlitz and D.J. Thouless, J. Phys. C **6**, 1181 (1973); J.M. Kosterlitz J. Phys. C **7**, 1046 (1974).

[2] J. Rogiers, T. Lookman, D.D. Betts, and C.J. Elliot, Can. J. Phys. **56**, 409 (1978); J. Rogiers, E.W. Grundke, and D.D. Betts, Can. J. Phys. **57**, 1719 (1979).

[3] M. Suzuki, S. Miyashita, A. Kuroda, and C. Kawabata, Phys. Lett. **60A**, 478 (1977); T. Onogi, S. Miyashita, and M. Suzuki, J. Stat. Phys. **45**, 1454 (1983).

[4] M. Suzuki, Prog. Theor. Phys. **56**, 1454 (1976).

[5] A recent analytical application of the ST transformation is: D.P. Aalberts and A.N. Berker, Phys. Rev. B **49**, 1073 (1994).

[6] H. DeRaedt, B. DeRaedt, and A. Lagendijk, Z. Phys. B **57**, 209 (1984); H. DeRaedt and A. Lagendijk, Phys. Rep. **127**, 233 (1985); T. Onogi, S. Miyashita, and

M. Suzuki, in *Quantum Monte Carlo Methods*, edited by M. Suzuki (Springer-Verlag, Berlin, 1987), p. 75.

[7] E. Loh, D.J. Scalapino, and P.M. Grant, Phys. Rev. B **31**, 4172 (1985).

[8] M. Marcu, in *Quantum Monte Carlo Methods*, ed. M. Suzuki (Springer-Verlag, Berlin, 1987), p. 64.

[9] H.-Q. Ding and M.S. Makivić, Phys. Rev. B **42**, 6827 (1990); H.-Q. Ding, *ibid.* **45**, 230 (1992); M.S. Makivić, *ibid.* **46**, 3167 (1992).

[10] H.F. Trotter, Proc. Am. Math. Soc. **10**, 545 (1959).

[11] The same argument has been made for the path integral formulation of the superfluid problem, see: R.P. Feynman and A.R. Hibbs, *Quantum Mechanics and Path Integrals* (McGraw-Hill, New York, 1965), Sec. 10-4.

[12] E.L. Pollock and D.M. Ceperley, Phys. Rev. B **36**, 8343 (1987); D.R. Nelson and J.M. Kosterlitz, Phys. Rev. Lett. **39**, 1201 (1977).

[13] M.S. Makivić and H.-Q. Ding, Phys. Rev. B **43**, 3562 (1991).

Chapter 3

Gels

In this chapter, I describe several calculations on the properties of gels. In Section 3.1, I use a recently developed Monte Carlo simulation technique to study the scaling properties of gels: I study Flory's supposition that free polymers behave in the same way as polymers in a gel. These are the first direct simulations of gels that I am aware of. In Section 3.2, I add to the simulation interactions between the gel and the solvent which lead to experimentally observed first-order phase transitions in ionic gels. In Section 3.3, we construct a Hamiltonian to model the quenched random Coulombic interactions between monomer groups of different types in polyampholytic gels.

3.1 Gel Scaling Behavior

Determination of Scaling Exponents of Polymer Gels

Daniel P. Aalberts

Department of Physics, Massachusetts Institute of Technology, Cambridge, Massachusetts 02139, USA

Abstract

The scaling exponents of polymer networks in two and three dimensions are studied via the Bond Fluctuation Method. It is found that the distance between cross-links follows the scaling law for self-avoiding random walks, $R_L \sim N^\nu$, and that the volume of the gel scales like R_L^d which confirms a supposition of Flory.

PACS Numbers: 82.70.Gg, 64.60.Fr, 36.20.Ey, 36.20.Hb

Although numerical methods have proven useful for studying the statistical properties of polymer chains, they generally fail when forced to deal with branched polymers and gels. The kink-jump, crankshaft, bead-spring, and reptation Monte Carlo approaches [1] as well as Molecular Dynamics [2] simulations are means of generating statistical fluctuations in the positions of the chains while preserving excluded volume constraints. The recently developed Bond Fluctuation Method (BFM) combines computational ease with the possibility of studying branched polymers and polymer-polymer interactions[3].

The BFM approximates a polymer as a bead necklace. Model polymers are composed of hard-core spheres tethered to give connectivity. The separation of tethered beads is constrained to lie within a maximum distance which prohibits, for a given bead size, chain crossings. The BFM has its roots in a paper on tethered surfaces [4] where a square-well potential between connected spheres was used. In that work, a bead could move a fixed distance in any of 4π steradians in each Monte Carlo Step (MCS). Carmesin and Kremer [3] discretized the spatial locations of the beads and achieved computational ease and the speed necessary to observe dynamics consistent with those predicted by the Rouse model [5]. BFM studies have been performed in two dimensions [3, 6, 7] and in three dimensions [3, 8, 9, 10, 11, 12]. The BFM also avoids many shortcomings of other numerical techniques such as trapped configurations and the inability to include cross-links. Thus, star polymers and gels are numerically accessible to the BFM.

In this paper, the scaling behavior of gels is studied using the BFM. Gels are simply networks of polymer chains. A convenient mental picture is that of a fishnet: the segments of rope (polymer chains) wriggle about but some topological order is preserved through the knots (cross-links). Scaling behavior is insensitive to small-scale details so the BFM should prove reliable even with simplifications such as discretization. Gels are an interesting class of materials which share properties with solids (global connectivity) and liquids (disorder). They are familiar to us as the dessert Jello, or as casings for medicines, or as the water absorbing element in modern diapers. Mean-field theories for gels were developed by Flory and Huggins [13] but

microscopic simulations were not previously possible.

The characteristic length scale $R_{\rm P}$ of polymers measures the average distance from end-to-end of the chain. It is well known that the random walk scales like

$$R_{\rm P} \sim N^{\nu}, \tag{3.1}$$

with $\nu = 1/2$ for an N-step walk. The non-intersection restriction of real chains tends to extend the walk leading to an increase of the exponent ν. Flory's mean-field theory estimate for self-avoiding random walks yields an exponent $\nu = 3/(d+2)$ Flory assumed that the chains, even in a gel, would scale with the same power law $R_{\rm L} \sim N^{\nu}$, where $R_{\rm L}$ is the distance between cross-links. The volume occupied by the gel would then scale as $V \sim R_{\rm L}^{d}$. These assumptions are at the heart of Flory's theory for gels [13] although the notation has since evolved [5, 15]. I use the BFM to study this supposition.

A gel is a network of chains interconnected by cross-links. A model gel of the type used in these simulations is depicted in Fig. 3-1. Cross-links form a topological lattice interconnected by chains of the same length. The networks considered have L repeating units per edge with $(n-1)$ beads separating nearest neighbor cross-links. Internal coordinate i gives the topological location of a bead while the spatial coordinate of bead i is given by $\mathbf{r}_i$. In addition, a logical array marking the positions of the beads in physical space is stored as $S(\mathbf{r})$. The memory requirements of storing the three-dimensional array $S(\mathbf{r})$ ultimately limit the gel sizes considered.

The simulation is carried out by randomly choosing a bead i and a direction for a move of unit length. The move is accepted if, at the new position, it does not make the bead overlap with another nor violates the tethered-bead constraint for the neighboring sites. Cross-link moves are attempted d times per MCS to improve diffusivity of these highly constrained points.

For significant improvements in computation time, the hard-core exclusion condition is evaluated by logical **or** operations on $S(\mathbf{r}_{hc})$ for all sites $\mathbf{r}_{hc}$ which would be prohibited by the new position. In two dimensions, with a bead size of $\rho_{min}^2 = 4$, this

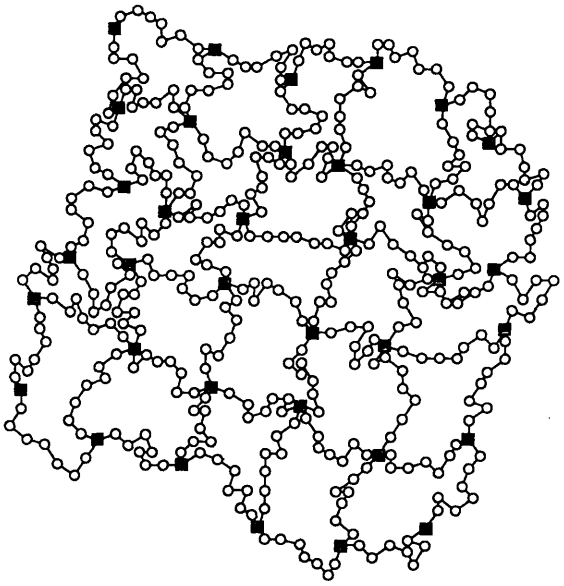

Figure 3-1: Configuration for a model two-dimensional gel. The number $(n-1)$ of beads in a chain is 7. The number of unit cells on each side L is 5. Cross-links are depicted with gray boxes.

amounts to checking if there is a bead in any one of the three sites in which beads might overlap — violating the hard-core exclusion — if the bead move were allowed. In three dimensions, with beads of $\rho_{min}^2 = 9$, this amounts to checking twenty-five sites.

The tethering constraint can be implemented for any bead size ρ_{min}. Table 3.1 lists pairs of values for ρ_{min} and ρ_{max} which prevent chains from crossing in two or three dimensions. Some work has appeared in the literature [8, 14] with values

ρ_{min}^2	1	2	3	4	5	6	8	9
ρ_{max}^2 $(d=2)$	2	10	-	13	20	-	34	34
ρ_{max}^2 $(d=3)$	2	3	8	8	10	14	16	18

Table 3.1: Self-consistent tethered-bead conditions in $d = 2,3$: $\rho_{min}^2 \leq |r|^2 \leq \rho_{max}^2$

inconsistent with Table 3.1 and therefore allows polymer chains to pass through one another. While this "phantom chain" approach may allow interacting polymers to find ground states more readily in a simulated annealing for random ionic interactions,

it violates the topological constraint of a real chain. Deutsch [12] is able to use a larger ρ_{max} than in Table 3.1 by imposing, somewhat arbitrarily, an additional constraint prohibiting a collection of latice vectors with $r < \rho_{max}$. For the simulations in three dimensions, I chose to work with $\rho_{min} = 3$ in order to allow for "inchworm" diffusion: beads are allowed to separate by a unit thus allowing for direct translational motion rather than merely rotations around bond angles.

Data is taken after a number τ_0 of Monte Carlo Steps. In the characteristic time, $\tau_0 = (bnL)^2$ MCS, a bead would diffuse the length of the sample via random walk dynamics if unimpeded by the constraints of the network[4]. The distance between neighboring beads b is taken to be the integer value in the center of the square-well potential; in this work $b = 3$ for both dimensionalities presented here. Since τ_0 is the decay time for the spatially longest — and thus slowest — decay mode in the Rouse model [5], when averages are computed, independent configurations should be guaranteed.

The order parameters studied are: *(i)* the area in $d = 2$ (volume in $d = 3$) and *(ii)* the average distance R_{L} between cross-links. In two dimensions, the area is calculated by summing up the contributions from each bead on the perimeter. This is done by calculating the cross products of the vector from the center of mass to a bead on the network's perimeter and the vector connecting that bead to its neighbor. The total area for a gel in the xy-plane is:

$$A = \sum_s \frac{1}{2} \left[(\mathbf{R}_s - \mathbf{R}_{\mathrm{COM}}) \times (\mathbf{R}_{s+1} - \mathbf{R}_s) \right] \cdot \hat{z}, \tag{3.2}$$

where $\mathbf{R}_s$ labels beads on the gel's surface, its perimeter, with s increasing counter-clockwise and $\mathbf{R}_{\mathrm{COM}}$ defines the position of the center of mass.

In three dimensions, the volume was estimated by locally computing the volume of the polyhedron formed from the lattice of cross-link points that compose the surface of the network. Local volumes ΔV of tetrahedra are determined using three vectors — one from the center of mass to the surface point and two from the surface point

to nearest neighbor surface points — and taking the vector triple product:

$$\Delta V = \frac{1}{6}[(\mathbf{R}_{s'} - \mathbf{R}_s) \times (\mathbf{R}_{s''} - \mathbf{R}_s)] \cdot (\mathbf{R}_s - \mathbf{R}_{\mathrm{COM}}), \tag{3.3}$$

where the subscript s labels a cross-link point on the surface and s' and s'' label neighbor cross-link points. The total volume is calculated by summing over all ΔV contributions. This summation scans the surface twice so one must divide by 2 to correct for this double counting.

The scaling results of the gel simulations for the cross-link distance R_{L} are given in Fig. 3-2. The scaling of R_{P} of free polymer chains is also given for comparison in Fig. 3-2 to indicate the effect of the network. Values for the exponents ν derived from Fig. 3-2 are plotted in Fig. 3-3 as a function of system size.

Flory assumed that cross-linking would leave the distribution of end-to-end vectors unchanged; Fig. 3-3 indicates, however, that without the topological constraint of crosslinking, free polymer chains scale with a somewhat (5%) smaller exponent. Overall, corrections due to the network are relatively small.

This 5% effect can be qualitatively understood by realizing that there is a higher than average density around the cross-links which will straighten the chains locally. Increasing the number of chains meeting at cross-links should make that effect more pronounced. In addition, the influence of nearby chains will tend to reduce perpendicular deviations and enhance the length. Another possibility is that the scaling exponent of a self-avoiding random *loop* differs from that of a self-avoiding random *walk*.

Another effect of the network is the growth of the effective chain link (the intercept in Fig. 3-2) with greater system size L. As L increases, so does the fraction of chains in the interior of the gel relative to those on the surface. Perpendicular fluctuations are more inhibited for interior chains because the density of beads is higher on all sides. Because the density of beads near interior crosslinks is greater than on the surface, chains will tend to be straighter.

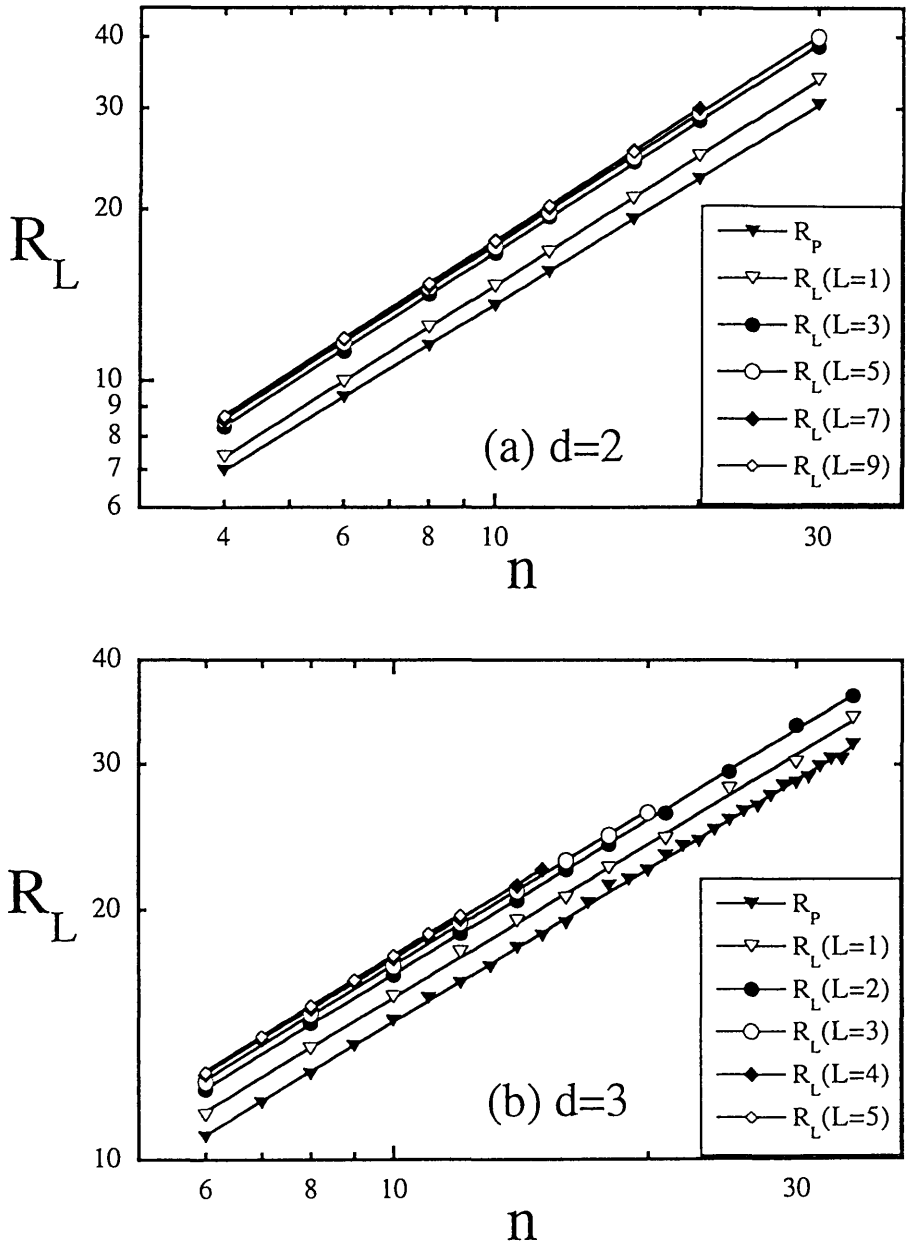

Figure 3-2: Scaling data for the distance between cross-links R_L from the Monte Carlo simulation. Data are given for gels and chains in (a) two dimensions and (b) three dimensions. Points are typically generated with $50\tau_0$ MCS, sampling every $\tau_0 = (3Ln)^2$ MCS, after discarding $10\tau_0$ MCS.

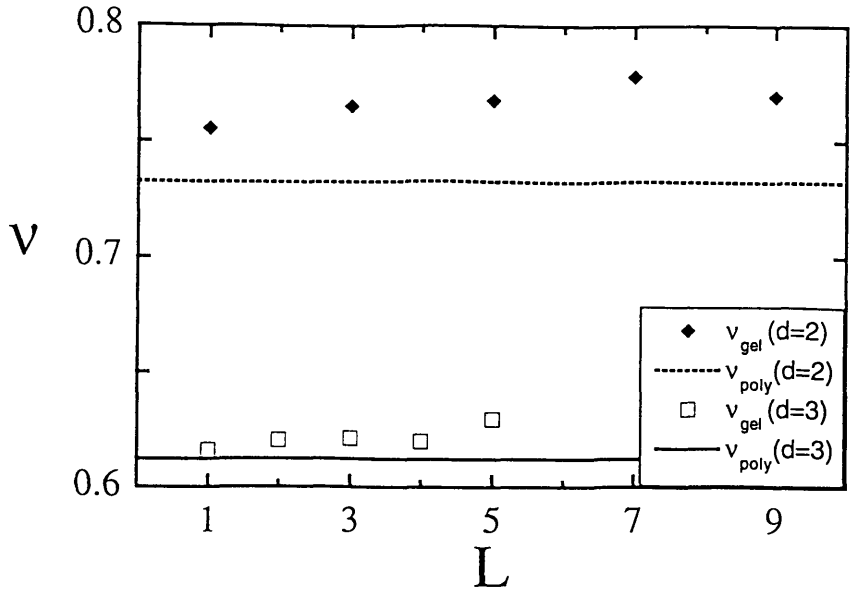

Figure 3-3: Scaling exponents derived from Fig. 3-2 plotted as a function of L, where L^d is the number of unit cells in the gel.

Figure 3-4 demonstrates that the data is consistent with $V \sim R_L^d$ for $d = 2$. Deviations observed for $d = 3$ where $V \sim R_L^{(2.925 \pm 0.004)}$ may be due to the small size of the systems although no systematic dependences were observed as L was varied.

Flory-Huggins theories for gels [13] generally assume gaussian exponents ($\nu = 1/2$) but these simulations clearly indicate self-avoiding walk exponents are nearer the mark. These data indicate the scaling regime extends to short chains.

The effect of random cross-linking and dangling ends on the exponents observed could be interesting because the scaling exponent might change. At low densities, polymers are well separated from one another and self-avoiding random walk exponents characterize end-to-end distances; at high densities, chains eventually interpenetrate and gaussian scaling is observed [15]. P.-G. de Gennes hypothesized that gels are at the overlap threshold for polymer chains [5] so the presence of extra chains could lead to cross-over of ν to a more gaussian character.

Interactions with the solvent lead to first-order phase transitions in real gels. Simulations have recently been completed on these interacting systems [16].

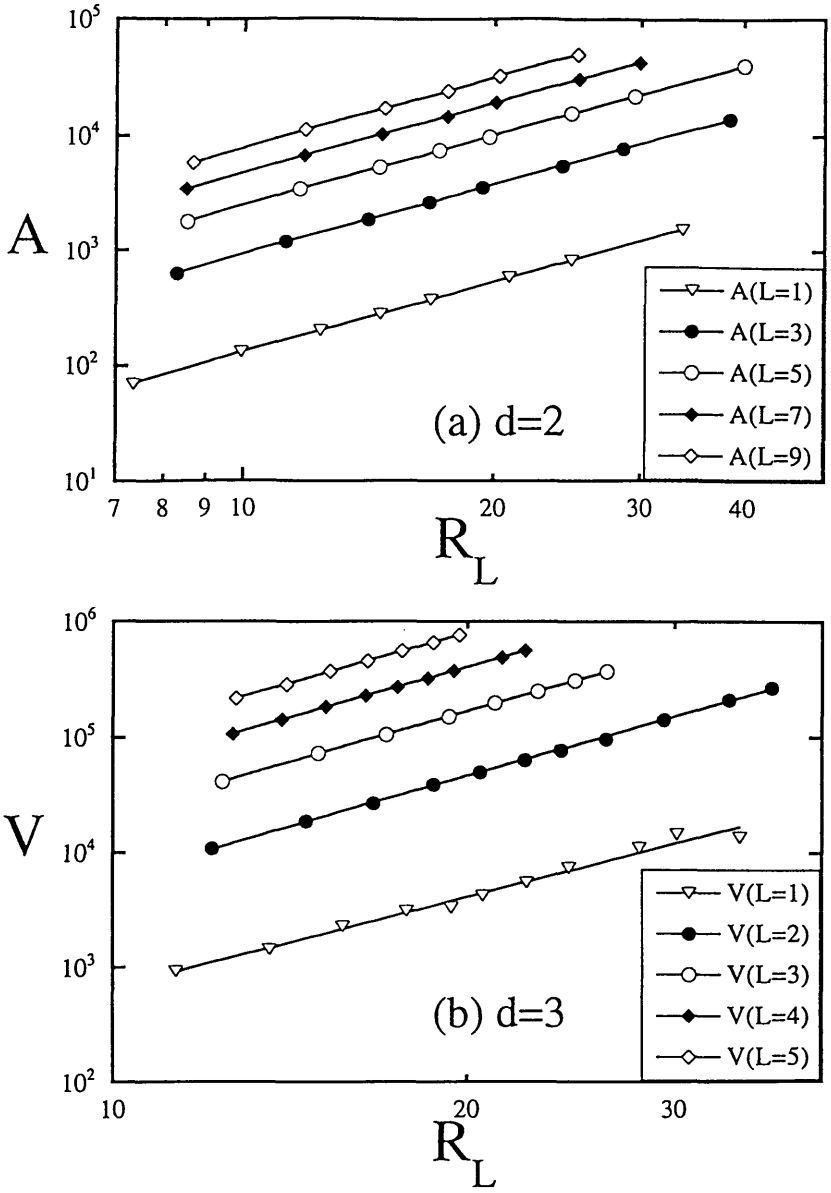

Figure 3-4: As a function of R_L: (a) the area of two-dimensional gels, and (b) the volume of three-dimensional gels.

I thank A. Nihat Berker for insights into scaling theory and for a critical reading of the manuscript. I am grateful to Yakov Kantor for helpful discussions. This work was supported by the US National Science Foundation Grant No. DMR-90-22933.

References

[1] A. Baumgärtner, *Applications of the Monte Carlo Method in Statistical Physics*, Ch. 5, ed. K. Binder (Springer, Berlin, 1987).

[2] See for example: G. Grest, K. Kremer, S.T. Milner, and T.A. Witten, Macromolecules **22**, 1904 (1989); G. Grest and K. Kremer, Macromolecules **23**, 4994 (1990).

[3] I. Carmesin and K. Kremer, Macromolecules **21**, 2819 (1988).

[4] Y. Kantor, M. Kardar, and D.R. Nelson, Phys. Rev. Lett. **57**, 791 (1986).

[5] P.-G. deGennes, *Scaling Concepts in Polymer Physics* (Cornell Univ. Press, Ithaca, NY, 1979), chapter VI.

[6] I. Carmesin and K. Kremer, J. Phys (Paris) **51**, 915 (1990).

[7] R. Dickman and P.E. Anderson, J. Chem. Phys. **99**, 3112 (1993).

[8] W. Jilge, I. Carmesin, K. Kremer, and K. Binder, Macromolecules **23**, 5001 (1990).

[9] H.P. Deutsch and K. Binder, J. Chem Phys. **94**, 2294 (1991).

[10] W. Paul, K. Binder, D.W. Heermann, and K. Kremer, J. Phys. (Paris) II, **1**, 37 (1991).

[11] H.P. Deutsch and R. Dickman, J. Chem Phys. **93**, 8393 (1990).

[12] H.P. Deutsch, J. Stat. Phys. **67**, 1039 (1992).

[13] P.J. Flory, *Principles of Polymer Chemistry* (Cornell Univ. Press, Ithaca, NY, 1953).

[14] Y. Kantor, M. Kardar, and H. Li, Phys. Rev. E **49**, 1383 (1994).

[15] P.-G. deGennes, *Scaling Concepts in Polymer Physics* (Cornell Univ. Press, Ithaca, NY, 1979), chapter II.

[16] D.P. Aalberts, MIT preprint, (1994). (Sec. 3.2 of this thesis.)

3.2 Interacting Gels

Microscopic Simulation of Phase Transition in Interacting Ionic Gels

Daniel P. Aalberts

Department of Physics, Massachusetts Institute of Technology, Cambridge, Massachusetts 02139, USA

Abstract

Gels are known to exist in expanded or collapsed phases. Interacting polymer networks are studied using the Bond Fluctuation Method in two dimensions. Two interactions — the quality of the solvent and the work done by a gas of counterions — suffice to characterize the first-order phase transition in these simulations. A technique is introduced which prevents local attractive interactions from hindering global relaxation. Simulation results are compared with Tanaka *et al.*'s experiments on ionic gels.

PACS Numbers: 82.70.Gg, 64.70.Fx, 36.20.-r, 5.70.Ln

First-order phase transitions in ionic gels have been observed experimentally by Tanaka *et al.* [1]. Unfortunately, until recently, numerical techniques only allowed for simulations of polymer chains. Cross-linking and other branching were not possible because connectivity constraints prevented cross-links from moving under the local symmetry operations which generate the statistical ensemble in the various techniques, namely, the kink-jump, crankshaft, and reptation, which are Monte Carlo approaches [2] as well as Molecular Dynamics [3] simulations are means of generating statistical fluctuations in the positions of chains while preserving excluded volume constraints. The invention of the Bond Fluctuation Method (BFM) changed this situation. Branching and cross-links can be included in the BFM [4]; thus, star polymers and gels are numerically accessible for the first time.

In this paper, I use the BFM to study the phase transition of gels, which are simply networks of polymers. I also introduce a method which prevents attractive interactions from inhibiting the global relaxation of the gel. Gels are an interesting class of materials used commercially to deliver drugs and make cement. Gels are also present in our eyes and joints. Mean-field theories for gels were developed by Flory and Huggins [5] but microscopic simulations have not been possible [6] until recently.

The BFM approximates a polymer as a bead necklace. The hard-core spheres of these model polymers exclude volume and the tethering constraint between connected beads enforces connectivity of the network. The separation r_{ij} between beads i and j must satisfy both the hard-core repulsion between beads and also the tethering constraint, if they are neighbors on a chain:

$$r_{ij} \geq \rho_{min}, \quad \text{for all pairs } ij, \tag{3.4}$$

$$r_{ij} \leq \rho_{max}, \quad \text{when } ij \text{ are chain neighbors.} \tag{3.5}$$

By constraining the separation ρ_{max} of connected beads for a given hard-core bead size ρ_{min}, chain crossings are prohibited [6]. The positions of the beads are discretized to a lattice in real space for computational efficiency [4]; for example, the hard-core calculation is simplified by storing bead positions in a logical array and by using

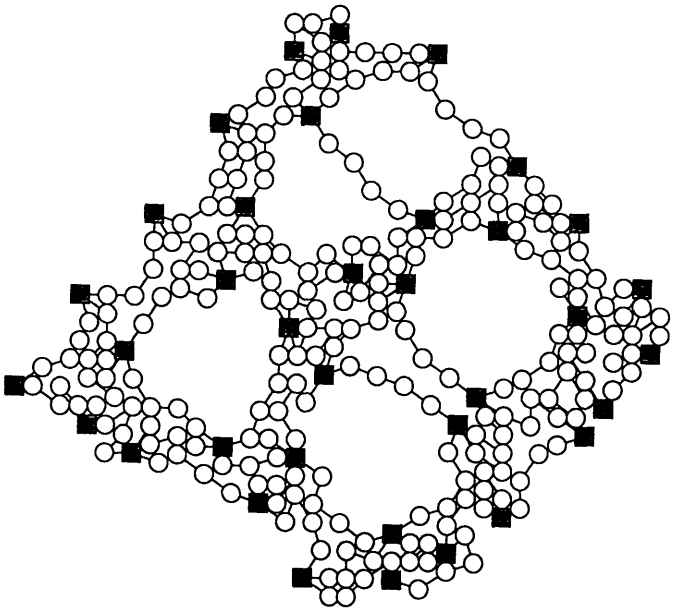

Figure 3-5: Configuration for an interacting gel in two dimensions. $n-1=4$ is the number of beads in a chain. $L=5$ is the number of unit cells on a side. Polymer-polymer coupling $J_P=-2$ and hydrogen ion coupling $J_H=5$ are used. Cross-links are depicted with shaded squares.

tables for distances. BFM studies have been performed for polymer chains in two dimensions [4, 7] and in three dimensions [4, 9, 10, 11, 12, 13] and for gels in two and three dimensions [6].

A gel network is a collection of chains interconnected by cross-links. The gel in this simulation is constructed with chains of the same length connected at cross-links where four chains intersect, except on the boundary. A convenient mental picture of the two-dimensional gel is that of a fishnet: the segments of rope (the polymer chains) can wriggle around but some global topological order is maintained by the knots (the cross-links). The networks considered (shown in Fig. 3-5) were composed of $(L+1)^2$ cross-links in a spatially fluctuating array topologically equivalent to a sqare lattice connected by chains with $(n-1)$ beads between cross-links.

Assuming no interactions between the chains in the network the decay time, in Monte Carlo Steps (MCS), of the slowest mode in the Rouse model [8, 14] is

$$\tau_0 = (bnL)^2, \tag{3.6}$$

where b is a characteristic distance between neighboring beads. When $\rho_{min} = 2$ and $\rho_{max} = \sqrt{13}$, this characteristic distance is taken to be $b = 3$. With averages computed after τ_0 MCS, statistically independent configurations should be guaranteed.

In every MCS, a move for each bead is attempted once (twice for cross-links to improve the diffusivity of these more highly constrained beads). In each move, the bead and the direction of the move of unit length are randomly selected. One must check to make sure the proposed position does not make the bead overlap with any other bead and that the tethered-bead constraint for the neighboring sites is not violated. If these constraints (Eqs. 3.4 and 3.5) are satisfied then one calculates the interaction energies and uses Metropolis sampling [2] to determine if the move is accepted.

Two interactions are considered. The first measures the relative affinity of a chain to be surrounded by solvent as opposed to by other polymers and is called the polymer-polymer interaction. The second is the work done to electrically confine the gas of counter-ions in the solvent to the volume of the gel and is called the hydrogen ion pressure.

Experimentally, the quality of the solvent is varied by altering the relative fraction of water and acetone which compose the solvent [1]. The polymer-polymer interaction gives the relative preference for a bead to sit next to solvent or some other bead. In the simulation, other beads j within a thin shell around the bead i, such that

$$r_{ij} \leq \rho_P, \tag{3.7}$$

are subject to J_P. The radius of the shell is taken to be the tethering radius,

$$\rho_P = \rho_{max}, \tag{3.8}$$

so tethered beads are always within ρ_P; thus, tethered beads do not effect the dynamics of the solution since in each valid bead-move there is no change in the interaction energy due to tethered beads.

The second interaction is the hydrogen ion term. In the experiments of Tanaka *et al.* [1], the gels are composed of chains with varying acidic monomeric unit concentrations. For the experiments, acrylamide gels were made and then by base-catalysed hydrolysis, monomers of acrylamide were slowly converted to monomers of acrylic acid ($-CONH_2$ to $-COOH$). Acrylamide has a pK_a of about 15 but acrylic acid has pK_a of 4.5. By definition, when pH = pK_a, half of the species is in the ionized form (A^- plus free H^+ ion) and the other half is neutral (AH). The experiments were carried out at a neutral pH of 7, where acrylic acid is generally ionized while acrylamide is generally neutral.

The degree of ionization affects the dynamics of the gel because the counter-ions of the acid (H^+) are confined by coulomb interactions to the volume occupied by the gel. Inside the gel, the charge of the hydrogen ions is compensated by the uniform background of negative charge of the ionized acrylic acid monomer A^-. When an H^+ tries to leave the volume of the gel, the coulomb force pulls it back inside. By Newton's third law, this force acts on the surface of the gel and is known as the hydrogen ion pressure.

To a first approximation, hydrogen ions behave like an ideal gas confined to a volume V or, for the two dimensional case considered here, an area A. The work ΔW done against this pressure contributes the hydrogen ion part of the Boltzmann weight

$$\Delta W = \frac{-N_{H^+} k_B T}{A} \Delta A, \tag{3.9}$$

$$\Delta(-\beta \mathcal{H}_H) = J_H C_0 \frac{\Delta A}{A}, \tag{3.10}$$

where $\beta^{-1} = k_B T$ and the normalization factor

$$C_0 = \frac{4 N_{\text{beads}}}{2n} \tag{3.11}$$

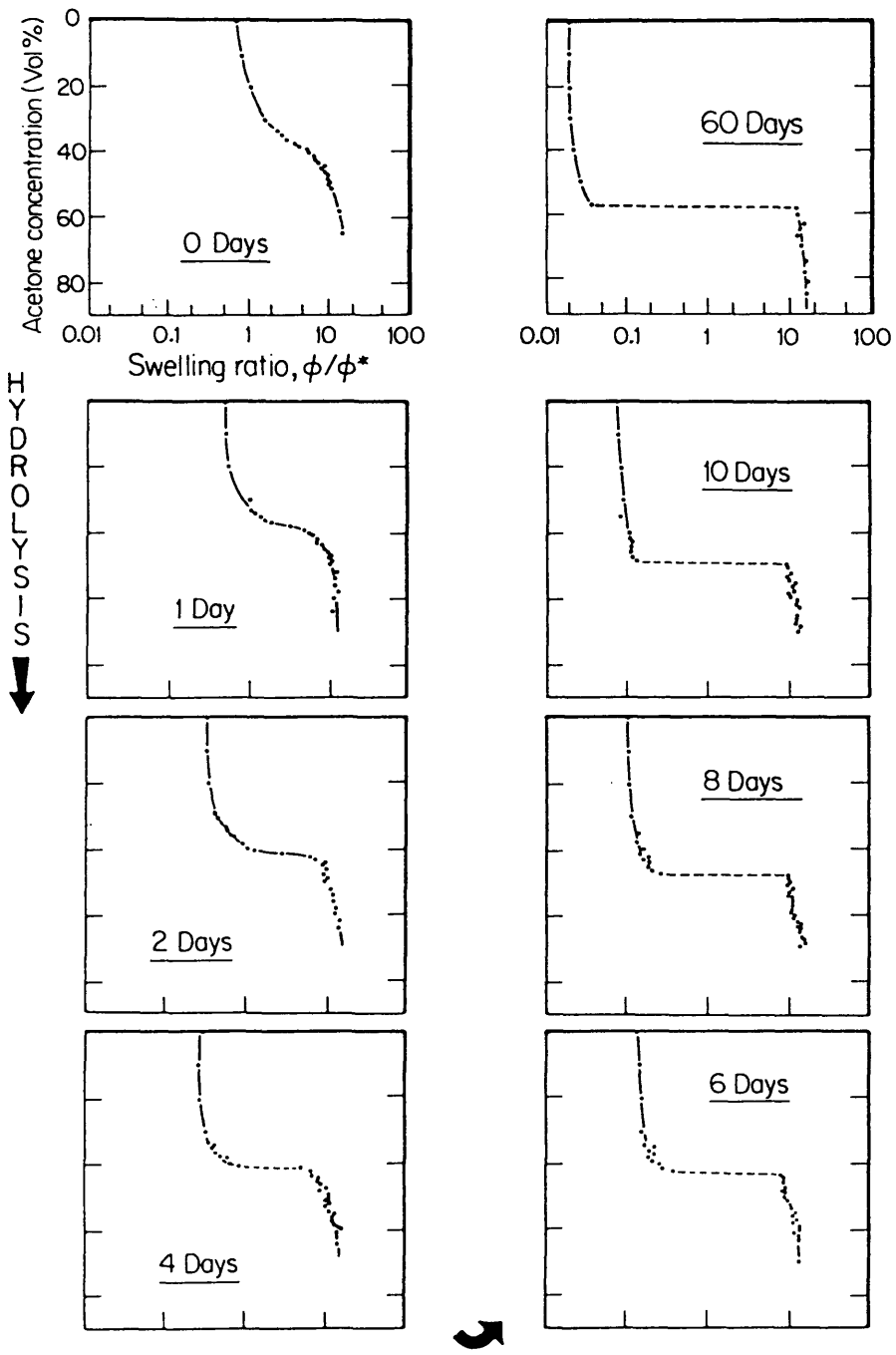

Figure 3-6: Experimental data from Ref. [1]. The acetone concentration dependence of the swelling ratio, $\phi/\phi^* \sim (\text{Volume})^{-1}$, for increasing hydrolyzation of the gel network. All curves are for gels immersed in 0.4% (volume) TEMED solutions for the times indicated, except for the upper right-hand plot, which is for gels immersed in a 4% (volume) TEMED solution for 60 d.

is constructed, for $\rho_{min} = 2$, to be the minimum area the gel can occupy divided by the largest ΔA for close-packed beads.

In this work, the hydrogen ion pressure Boltzmann weight [Eq. (3.10)] is calculated whenever a surface crosslink move is attempted. This approach is not necessary in $d = 2$ because the chains compose a well-defined surface but may be generalized to $d = 3$. The surface of a gel in three dimensions cannot be defined locally because of the large holes between the chains at the surface of the gel; however, the cross-links form a topological array which makes it possible to define a simply-connected surface — one without holes — for this lattice of branch points.

If one conducts the simulation as described above, in the region where $J_P < J_P^{crit}$, ergodically trapped close-packed configurations result. The system phase separates into two phases: one dense, the other dilute. Chains are stretched out completely in the dilute phase hence the beads will not be drawn closer together by enhancing the binding strength. This scenario, while exhibiting two-phase coexistence familiar in first-order phase transitions, also indicates a failure in the simulation technique to ergodically sample the equilibrium. The underlying assumption of a uniform background of negative charges in the gel is also violated by two-phase coexistence states.

Close-packed, tightly bound states are non-diffusive because there is an activation energy required to separate beads before the pair can move. This is clearly unphysical since there should be no impediment for large clusters to move, without the BFM's discretizing of space. One way to overcome this obstacle would have been to introduce cluster moves to the simulation; however, global connectivity constraints complicate implementing this approach.

Some degeneracy had to be built into the dense phase to compensate for these problems. To ensure diffusion, the number of beads benefitting from the local interaction energy J_P is capped at six. The contribution to the Hamiltonian for the polymer-polymer interaction is:

$$-\beta\mathcal{H}_P = -J_P \sum_i \min(6, \mathcal{N}_i), \tag{3.12}$$

where $\mathcal{N}_i$ is the number of beads within a distance ρ_P of bead i. The cap on the number interacting is reasonable on physical grounds as well: in close packed systems in two dimensions there are six nearest-neighbors. Without this cap, further-neighbors benefit from this interaction even though J_P measures the relative benefit of excluding solvent molecules which is a short range effect. In the simulation seven or more beads may come within ρ_P, but without additional energetic benefit; with the cap, beads tend to be spaced further apart, and diffusivity improves.

Since the beads on the perimeter form a simply connected surface in the xy-plane, the area was calculated by summing up contributions from each bead on the surface

$$A = \sum_s \frac{1}{2} \left[(\mathbf{R}_s - \mathbf{R}_{\mathrm{COM}}) \times (\mathbf{R}_{s+1} - \mathbf{R}_s) \right] \cdot \hat{z}, \tag{3.13}$$

where $\mathbf{R}_s$ label sequence of points on the gel's surface with s increasing counter-clockwise around the perimeter and where $\mathbf{R}_{\mathrm{COM}}$ is the position of the gel's center of mass.

The results of the gel simulations for $L = 5$ and $n = 5$ are given in Figs. 3-7 and 3-8. In Figure 3-7, the polymer-polymer interaction J_P is scanned for various fixed hydrogen ion coupling J_H. Hysteresis loops indicate first-order transitions and are observed for $J_H \gtrsim 8$. In Figure 3-8, J_P is held fixed while J_H is varied: Phase separation is evident for $J_P \lesssim -2$. Quantitative agreement between values for the area obtained by scanning in each direction confirms that thermodynamic minima have been found.

This work is the first use of the BFM to study phase transitions in cross-linked material. A method was introduced for interactions of a bead with its surroundings which prevents the system from getting "stuck" and allows it to find the global minima. To generalize to three dimensions, it is important to use minimally $\rho_{min} = 3$ in order to allow for "inchworm" diffusion of bound beads leading to global relaxation [6].

I thank A. Nihat Berker for suggesting this problem and for critical reading of the manuscript. This work is supported by the US National Science Foundation Grant No. DMR-90-22933.

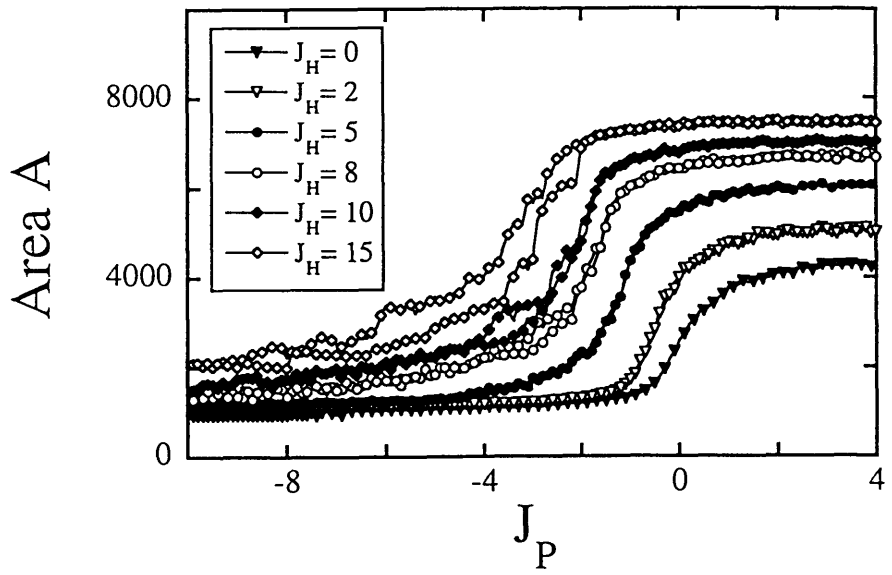

Figure 3-7: Area plotted varying the polymer-polymer interaction strength J_P at fixed hydrogen ion pressure J_H for $L = 5$, $n = 5$ gels in two dimensions. The hysteresis loops indicate a discontinuous (first-order) phase transition for $J_H \gtrsim 8$. Points are generated with $10\tau_0$MCS, after discarding $5\tau_0$MCS, sampling every $\tau_0 = 5625$ MCS.

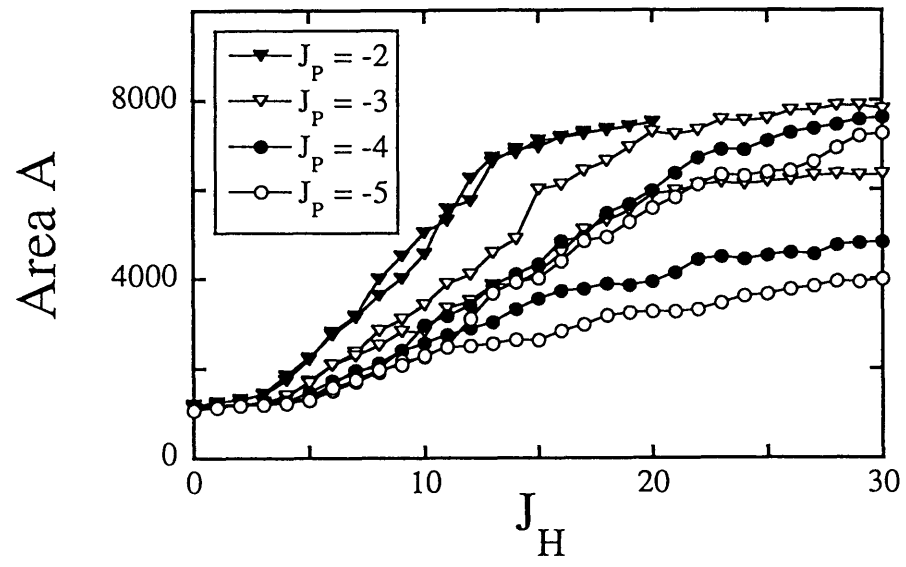

Figure 3-8: Area plotted varying the hydrogen ion pressure at fixed polymer-polymer interaction strength for $L = 5$, $n = 5$ gels in two dimensions. Data is plotted in the phase separation region. There is no phase separation for $J_P = -2$, indicating this is above the critical point. Phase separation increases as binding becomes stronger ($J_P < -2$). Points are generated with $10\tau_0$ MCS, after discarding $5\tau_0$ MCS, sampling every $\tau_0 = 5625$ MCS.

References

[1] T. Tanaka, D. Fillmore, S.-T. Sun, I. Nishio, G. Swislow, and A. Shah, Phys. Rev. Lett. **45**, 1636 (1980).

[2] A. Baumgärtner, *Applications of the Monte Carlo Method in Statistical Physics*, Ch. 5, edited by K. Binder (Springer, Berlin, 1987).

[3] See for example: G. Grest, K. Kremer, S.T. Milner, and T.A. Witten, Macromolecules **22**, 1904 (1989); G. Grest and K. Kremer, Macromolecules **23**, 4994 (1990).

[4] I. Carmesin and K. Kremer, Macromolecules **21**, 2819 (1988).

[5] P.J. Flory, *Principles of Polymer Chemistry* (Cornell Univ. Press, Ithaca, NY, 1953).

[6] D.P. Aalberts, MIT preprint (1994). (Sec. 3.1 of this thesis.)

[7] I. Carmesin and K. Kremer, J. Phys (Paris) **51**, 915 (1990).

[8] Y. Kantor, M. Kardar, and D.R. Nelson, Phys. Rev. Lett. **57**, 791 (1986).

[9] W. Jilge, I. Carmesin, K. Kremer, and K. Binder, Macromolecules **23**, 5001 (1990).

[10] H.P. Deutsch and K. Binder, J. Chem Phys. **94**, 2294 (1991).

[11] W. Paul, K. Binder, D.W. Heermann, and K. Kremer, J. Phys. (Paris) II, **1**, 37 (1991).

[12] H.P. Deutsch and R. Dickman, J. Chem Phys. **93**, 8393 (1990).

[13] H.P. Deutsch, J. Stat. Phys. **67**, 1039 (1992).

[14] P. G. deGennes, *Scaling Concepts in Polymer Physics* (Cornell Univ. Press, Ithaca, NY, 1979), chapter VI.

3.3 Polyampholyte Gels

High-Degeneracy Ordering of Polyampholyte Gels from a Random-Field Model

Daniel P. Aalberts and A. Nihat Berker

Department of Physics, Massachusetts Institute of Technology, Cambridge, Massachusetts 02139, USA

Abstract

Recent experiments by Annaka and Tanaka have yielded multiple coexistence loops for gels with random positive and negative ionic groups, demonstrating the existence of up to seven distinct macroscopic phases distinguished by volume discontinuities. We introduce for this system a microscopic model in which the randomness translates into random fields resulting in competing quenched random interactions in a spin system. The model yields the multiple coexistence of phases, as well as volume versus excess charge curves, similar to the experimental results. The many phases can be understood as randomly coordinated phases.

PACS Numbers: 82.70.Gg, 61.25.Hq, 75.10.Nr, 87.15.Da

Gels have been known to undergo a phase transition between a swollen and a collapsed phase [1]. Recently, many additional phases have been discovered by Annaka and Tanaka [2] in gels with random positive and negative ionic monomer groups. These phases are distinguished from each other and from the usual swollen and collapsed phases by density and local environment [2-4]. At the same final pH and temperature, depending on the path taken to that point in thermodynamic phase space, a multiplicity of phases is observed. In this paper, we develop a microscopic model for this phenomenon. The microscopic physical picture of this system leads to a spin model with two types of local degrees of freedom, coupled by competing quenched random interactions due to random fields. This spin model yields the multiple coexistence phenomena. The many phases can be understood as randomly coordinated phases. The model also yields volume versus charge curves in qualitative agreement with experiment [5] and another type of theory [6, 7].

The measurements of diameter versus pH on gels with diferent ratios of acrylic acid (the anionic group) and MAPTAC (methyl-amido-propyl-trimethyl ammonium chloride, the cationic group) share a general feature [2]: As pH is changed from either extreme toward neutral, a large jump occurs from the swollen phase to the collapsed phase; as the pH is changed from neutral toward either extreme, many smaller jumps occur as the gel expands.

The microscopic picture of these systems is as follows. The gel is composed of crosslinked polymer chains that contain random sequences of ionic groups. In a very acidic (basic) solution, the anionic (cationic) groups are neutralized and the cationic (anionic) groups are ionized; therefore, the gel swells from self-repulsion [6], although this repulsion is somewhat screened by the excess opposite charge in the solvent. As the pH is brought toward neutrality, both groups become partially ionized. Opposite charges can bind randomly across the gel, which lowers the energy and the entropy; the reduction of entropy arises from restricting the self-avoiding random walk of polymers.

We now build a model for these systems. The gel is modelled by volume elements i arranged as a simple cubic lattice. Each volume element, referred to as a site from

here on, is randomly assigned a net cationic or anionic character. For a cationic (anionic) site i, the local variable $q_i = +1$ (-1) or 0 denotes, respectively, ionized or neutralized states. This amounts to a spin-1 Ising (Blume-Emery-Griffiths) model [8] under a random field randomly suppressing one of the magnetized states at each site. The relative abundance of ionized or neutralized states is controlled by the pH, which equals the ionization reaction constant pK_a (pK_b) of an acid (base) when half the substance is ionized and half is neutral in the absence of other interactions. This contribution to the Hamiltonian can be expressed as

$$-\beta\mathcal{H}_{\rm pH} = \textstyle\sum_i \Delta_i q_i, \tag{3.14}$$
$$\Delta_i = (T_0/T)({\rm pH} - {\rm pK_a}) \ \text{ and } \ \Delta_i = (T_0/T)({\rm pK_b} - {\rm pH}),$$

for cationic or anionic components, respectively, where $T_0 = 298$ is the standard temperature and T is the actual temperature.

In the gel, charges interact via the Coulomb potential. In this model, the first way in which the Coulomb interaction manifests itself is that oppositely ionized neighboring sites can bind. The local variable $b_i = 1$ (0) denotes, respectively, that the site i is bound (unbound) to another nearby site. When a bond forms, the charges involved offset each other, thereby neutralizing their interactions with other charges. Thus, each site can participate in only one bond, so that the $b_i = 1$ states occur in pairs. We take a bond to be possible between a site and its six nearest neighbors, twelve second neighbors, and eight third neighbors. In other words, all of the sites within a $2 \times 2 \times 2$ unit cell mutually interact and each site participates in eight unit cells. This contribution to the Hamiltonian can be expressed as

$$-\beta\mathcal{H}_{\rm bind} = \sum_i J_{\rm B} b_i, \tag{3.15}$$

where $2J_{\rm B} > 0$ is the binding energy. Since binding contracts the gel, a normalized measure of volume is

$$v = 1 - \langle b_i \rangle. \tag{3.16}$$

Another way in which the Coulomb potential manifests itself is by the interaction of nearby but unbound charges. Such a contribution to the Hamiltonian can be expressed as

$$-\beta\mathcal{H}_{\rm Coul} = \sum_{\mu}\sum_{ij}^{\mu}(J_0 - J_1 b_\mu)q_i q_j(1-b_i)(1-b_j), \tag{3.17}$$

where the first sum is over the unit cubes μ, the second sum is over the sites of each unit cube, and b_μ is the number of bound pairs within cube μ. The occurence of two opposing terms, with interaction constants J_0 and J_1, allows for the drastically different local environments of expansion and contraction. On the one hand, in the absence of bound pairs ($b_\mu = 0$), the local gel is expanded and envelopes the counterions from the solution. If the unit cube is populated by like charges, it will admit counterions of the opposite sign and be in an energetically favorable state. If the unit cube is populated by unlike charges, the counterions will interact with their like charges on the gel and cause an energetically unfavorable state. On the other hand, in the presence of bound pairs ($b_\mu > 0$), the local gel is contracted and its charges interact directly, energetically favorably for unlike charges and vice versa. The higher the number of bound pairs b_μ, the more contracted is the gel, with the interaction getting stronger as $J_1 b_\mu$.

Thus, the complete Hamiltonian is

$$-\beta\mathcal{H} = \sum_{\mu}\sum_{ij}^{\mu}(J_0 - J_1 b_\mu)q_i q_j(1-b_i)(1-b_j) + \sum_i(\Delta_i q_i + J_{\rm B} b_i). \tag{3.18}$$

In the determination of b_μ, the contribution of a bound pair belonging to several unit cubes is shared by the latter, so that edge, face-diagonal, and body-diagonal pairs respectively contribute $\frac{1}{4}$, $\frac{1}{2}$, and 1 to each μ. We have studied the model defined by the Hamiltonian of Eq. (3.18) using Monte Carlo simulation and have found that the distinctive qualitative features of the polyampholyte gel experiments are reproduced. Data is shown below at 33% MAPTAC concentration, with which the largest number of distinct phases was observed experimentally [2, 3]. An $8 \times 8 \times 8$ system with open boundary conditions was simulated, with $J_{\rm B} = 2(T_0/T)$, $J_0 = 0.2(T_0/T)$, and $J_1 = 1.6(T_0/T)$.

To demonstrate the multiplicity of collapsed phases, the system at a given pH was annealed (heated and cooled) repeatedly. The systems at extremal pH are in the maximally expanded phase at lower temperatures, as seen for pH = 2.0 in Fig. 3-9(a) and pH = 15.0 in Fig. 3-9(e). The system at neutral pH = 7.0 is in the maximally collapsed phase at lower temperatures, as seen in Fig. 3-9(c). By contrast, the systems at intermediate pH indeed access, at lower temperatures, multiple phases with distinct partial collapses, when they are cycled up and down the temperature scale, as seen for pH = 2.4 in Fig. 3-9(b) and pH = 13.25 in Fig. 3-9(d).

Fig. 3-10(a) shows the volume of the gel as a function of the excess charge in the gel, $Q = \frac{1}{N}\sum_i q_i$, where N is the number of volume elements in the model. The characteristic flat bottom, sandwiched between the sharp rises, seen experimentally (Figs. 3-10(b,c) from Ref. [5]), is thus obtained from the model.

We have thus constructed a model Hamiltonian of coupled charge and binding degrees of freedom, based on microscopic phenomenology, that captures the qualitative behavior observed by Annaka and Tanaka in their experiments [2, 3] on polyampholyte gels. The model can be discussed in spin language: A random field on an $s = 1$ model induces a quenched random spatial distribution of possible opposite spin states that equilibrate with zero-spin states via the pH. The non-zero spins represent the ionized monomers and have alternate local binding configurations bringing together opposite pairs. As the occurrence of the up and down spins is changed via the pH, the system moves from maximal binding (collapsed gel) to non-binding (expanded gel). In between, in the partial binding regimes, the multiplicity of local binding configurations gives rise to a macroscopic diversity, namely the coexistence of multiple phases with distinct partial collapses.

We thank Prof. Toyoichi Tanaka for many useful discussions. This research was supported by the US National Science Foundation Grant No. DMR-90-22933.

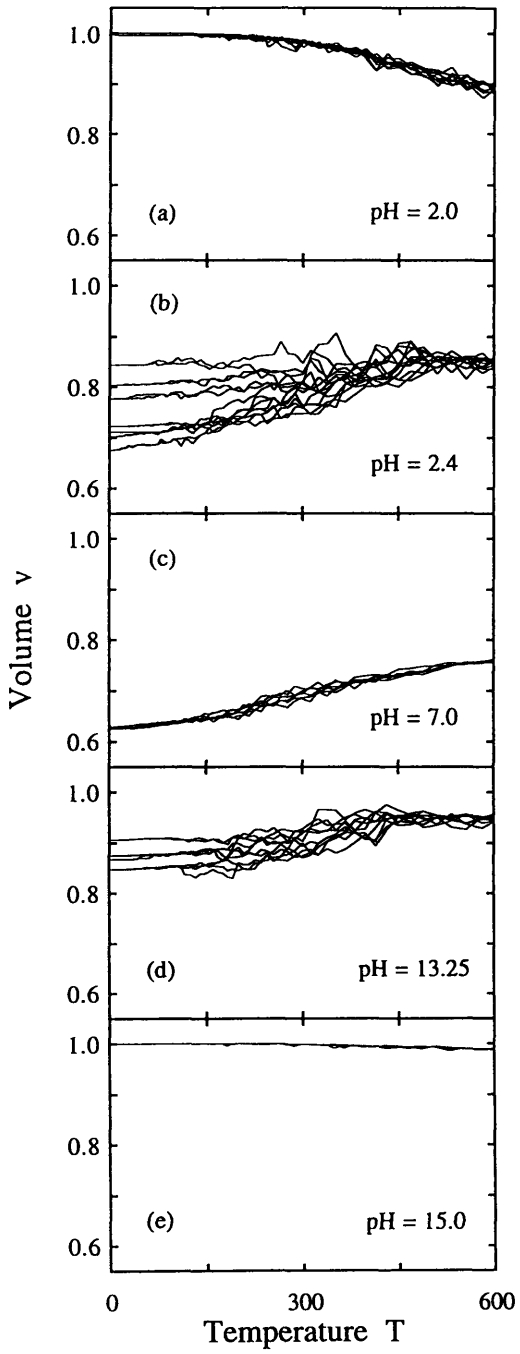

Figure 3-9: Gel volume as a function of temperature. For each pH, the system is repeatedly annealed (heated and cooled) in search of multiple phase coexistence, using $T/(T_0 + T)$ steps of 0.01 and, at each temperature, 200 (after discarding 100) Monte Carlo steps per spin. At intermediate pH (b,d), it is seen that multiple phase coexistence indeed occurs, with distinct partial collapses. For extremal pH (a,e) and neutral pH (c), the gel is in the totally expanded and collapsed phases respectively.

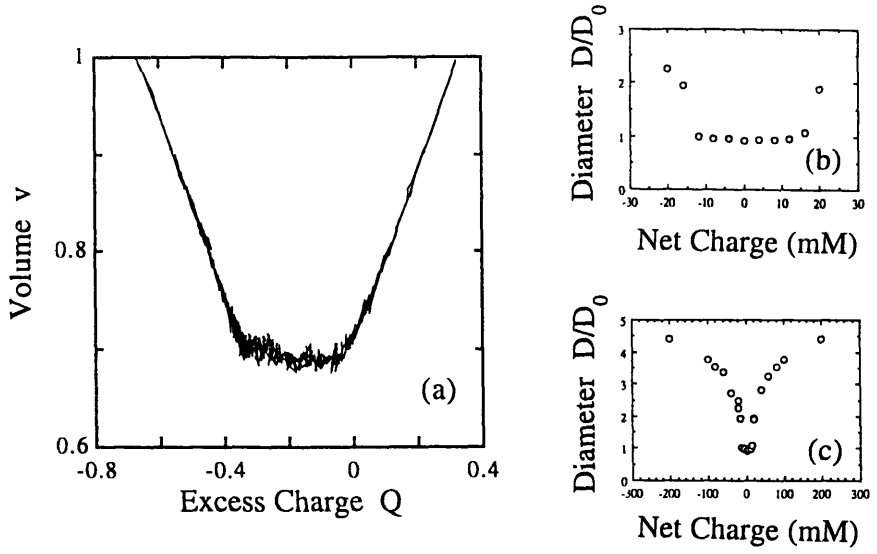

Figure 3-10: (a) Calculated volume as a function of net charge on the gel. (b,c) Experimental swelling degree of AMPS/MAPTAC copolymer gel as a function of net charge concentration, from Ref. [5].

References

[1] T. Tanaka, D. Fillmore, S.-T. Sun, I. Nishio, G. Swislow, and A. Shah, Phys. Rev. Lett. **45**, 1636 (1980).

[2] M. Annaka and T. Tanaka, Nature **355**, 430 (1992).

[3] M. Annaka and T. Tanaka, MIT preprint (1991).

[4] Refs. [2] and [3] appear to be the first observations of a gel phase transition driven by electrostatic interactions.

[5] X. Yu, Ph.D. thesis, MIT (1993).

[6] Y. Kantor and M. Kardar, Europhys. Lett. **14**, 421 (1991).

[7] Y. Kantor and M. Kardar, MIT preprint (1994).

[8] Hydrogen bonding, weaker than Coulomb binding, can pair anionic groups, but is not strong enough to drive the phase transitions considered here, as discussed in F. Ilmain, T. Tanaka, and E. Kokufuta, Nature **349**, 400 (1991).

[9] M. Blume, V.J. Emery, and R.B. Griffiths, Phys. Rev. A **4**, 1071 (1971).

Chapter 4

Conclusions and Future Prospects

In this thesis I have had the pleasure to work on two of the most interesting topics in statistical physics today: quantum systems and random systems. I developed new microscopic models and theoretical methods for the understanding of these systems.

There is much work still to be done in both topics.

In the topic of quantum statistical mechanics, two major thrusts come readily to mind. First, it would be most rewarding to learn how to construct renormalization group calculations for quantum systems. I believe that having a visual and intuitive picture for the transition like that developed in Chapter 2 is a key element towards that end. It would also be rewarding to study the cross-over between quantum and classical systems in order to understand better their relation to each other.

Second, both magnetic Hamiltonians studied in Chapter 2 have Bose-Einstein quantum statistics, meaning wavefunctions are even under particle exchange. Studying Fermionic systems (*i.e.*, electronic problems) in which exchanging particles leads to a minus sign for the wavefunction, adds another layer of complexity. This minus sign stymies Quantum Monte Carlo simulations and other theoretical approaches. Perhaps it is possible to invent ways of representing Fermionic systems using the Suzuki-Trotter mapping or some other technique which will make these problems more tractable.

Similarly, for the field of random systems, there are two major areas which deserve mention. Biological problems are receiving much attention because of the analogies

to statistical physics. In biology, one is interested in determining how competing atomic interactions lead to objects of biological import on larger and larger length scales: proteins, cells, organisms. In addition, it seems that the language of phase transitions may be helpful *(i)* to express how cells with the same genetic information can develop to serve such different functions as neurons, muscles, skin, and so on; and *(ii)* to characterize diseases such as cataracts, sickle-cell anemia, kidney stones, and Alzheimer's disease.

Finally, in systems with random competing interactions glassy states are often observed. Glassy states are those in which true thermodynamic equilibrium has not been reached but the system freezes into some deep local free energy minima. Among other applications, these kinds of systems have been used to model memory storage in the brain. Other interesting questions arise from their study: How do non-ergodic states occur? Can the limitations of the replica-symmetry breaking approach to solving these problems be overcome? Can some sort of scaling theory be constructed in which non-equilibrium properties are observed?

Biographical Note

Daniel Aalberts was born in Sioux Falls, South Dakota, on October 9, 1966. He grew up in Cedar Rapids, Iowa where he graduated as valedictorian of Jefferson Senior High School in 1985. He was, and remains, active in music and theater.

He attended the Massachusetts Institute of Technology majoring in physics. He was awarded the National Merit Scholarship and the IBM's Thomas J. Watson Scholarship. While an undergraduate, he performed with and directed the Logarhythms, a twelve-man *a cappella* ensemble and was an enthusiastic participant in intramural basketball and volleyball. He worked many summer and winter breaks for IBM. His bachelor's thesis "Modelling the Behavior of Relativistic Magnetrons" was done under the supervision of Professor George Bekefi and Dr. Shien-Chi Chen.

He spent two summers working at the Lawrence Livermore National Laboratory with the experimental Relativistic Klystron research group headed by Dr. Glen Westenskow.

While at MIT for doctoral studies as a National Science Foundation Fellow, he organized an *a cappella* quartet, The Strange Attractors; sang with the MIT Gospel Choir; was active performing lead roles and directing with the MIT Musical Theater Guild and MIT Dramashop; and performed solo vocal concerts. He also captained an A-league intramural basketball team. He served as Graduate Resident Tutor of East Campus' Second West hallway for four years. He taught recitation sections for three Independent Activities Period classes: "Phase Transitions and Renormalization-Group Theory;" "Neural Networks, Simulated Annealing, and Phase Transition Models;" and "Superconductivity;" and served as a teaching assistant for Graduate Quantum Mechanics.

He married Danielle Fogarty on June 4, 1993.

Beginning in September, 1994, he will work as a postdoctoral fellow at the University of Leiden.